INSTITUTE OF PHYSICS PUBLISHING REPORTS ON PROGRESS IN PHYSICS

Rep. Prog. Phys. **66** (2003) 691–736 PII: S0034-4885(03)69400-5

Dark matter, dark energy, gravitational lensing and the formation of structure in the universe

Francis Bernardeau

Service de Physique Théorique CEA/DSM/SPhT, Unité de recherche associée au CNRS, CEA/Saclay 91191 Gif-sur-Yvette Cédex, France

Received 15 January 2003
Published 15 April 2003
Online at stacks.iop.org/RoPP/66/691

Abstract

The large-scale structure of the universe and its statistical properties can reveal many aspects of the physics of the early universe as well as of its matter content during the cosmic history. Numerous observations, based to a large extent on large-scale structure data, have given us a concordant picture of the energy and matter content in the universe. In view of these results the existence of dark matter has been firmly established although it still evades attempts at direct detection.

An even more challenging puzzle is, however, yet to be explained. Indeed the model suggested by the observations is only viable with the presence of a 'dark energy', an ethereal energy associated with the cosmological vacuum, that would represent about two-thirds of the total energy density of the universe. Although strongly indicated by observations, the existence of this component is nonetheless very uncomfortable from a high-energy physics point of view. Its interpretation is a matter of far reaching debates. Indeed, the phenomenological manifestation of this component can be viewed as a geometrical property of large-scale gravity, or as the energy associated with the quantum field vacuum, or else as the manifestation of a new sort of cosmic fluid that would fill space and remain unclustered. Low redshift detailed examinations of the geometrical or clustering properties of the universe should in all cases help clarify the true nature of the dark energy.

We present methods that can be used in the future for exploring the low redshift physical properties of the universe. Particular emphasis will be placed on the use of large-scale structure surveys and more specifically on weak lensing surveys that promise to be extremely powerful in exploring the large-scale mass distribution in the universe.

0034-4885/03/050691+46$90.00

Contents

1. Introduction

During the last few years our views on the matter and energy content of the universe have evolved dramatically. A convincing picture has emerged recently in which it is possible to reconcile numerous observations and constraints of very different origin. Those observations are related to the determination of the matter content of the largest gravitationally bound objects that can be observed, namely galaxy clusters, to estimations of the ages of the oldest star populations, to observations of the large-scale structure of the universe, galaxy or dark matter surveys, anisotropies of the cosmic microwave background, and to the light dimming of distant supernovae.

The emerging picture is the following. Photons, together with neutrinos are probably by far the most numerous particles in the universe. Their energy density accounts, however, for a very small part of the total ($<10^{-4}$) because, having been considerably redshifted, those photons carry very little energy. They follow an almost perfect black body spectrum, whose temperature has now been measured with exquisite precision to be 2.725 K [73]. The case for the neutrinos is more complex since their mass could have had a significant impact on the fate of the universe. Recent observations of neutrino oscillations have shown that these particles were indeed massive [2, 1, 41]. However, the mass scales that have been inferred from these experiences are far below those of interest for cosmology. In the most favourable, but unlikely case, neutrinos cannot account for more than a few per cent of the total energy density. The present day constraint on the total mass of neutrinos is that it cannot exceed 1.8 eV [35].

The existence of baryonic matter cannot be doubted. However, all observations show that it cannot account for more than 30% of the mass encountered in objects like galaxy clusters. In those objects the intergalactic baryonic matter can indeed be observed because the gas is heated to a temperature such that it emits x-ray radiation in abundance. These observations clearly imply the existence of a large dark matter component, which should account for more than two-thirds of the matter content of the universe. In view of these results, the existence of dark matter is firmly established although it still evades attempts at direct detection.

The dark matter component, however, accounts only for about 25% of the energy density of the universe. Observations made over the recent years have indeed made it clear that a non-zero energy density associated with a so-called dark energy was needed. It can be identified with a mere cosmological constant or with a yet unknown matter state. This component is different from the pre-quoted dark matter in the sense that it remains unclustered. As a result, gravitational instabilities do not develop in this medium. It is, however, thought to be responsible for a general acceleration of the expansion of the universe because of a negative pressure. If it appears to be a reasonable picture from the point of view of observational cosmology, such a hypothesis is very challenging from a high-energy physics perspective. That such a cosmic component should exist is certainly one of the most puzzling findings of recent years.

One aim of this review is to scrutinize the evidence for the existence of dark matter and that for a dark energy component. The existence of this unknown form of matter raises many questions regarding its specific properties. We will explore what kind of observations could answer some of these questions. It appears, in particular, that the large-scale structure of the universe, and its statistical properties, could be used to reveal many aspects of the physics of the early universe as well as information on its matter and energy content. Mappings of the large-scale structure have provided a wealth of new results over the last few years whether it is from conventional galaxy surveys or from gravitational lensing surveys. The latter has already proved extremely powerful in mapping matter inhomogeneities at cosmological scales and appears very promising for the development of precision cosmology. We shall see how these surveys could be used in the future to explore our knowledge of gravitational physics at the Hubble scale.

The review is organized as follows. We first review the direct evidence for dark matter in astrophysical objects in section 2. We then present the standard model of the growth of structure from gravitational instability dynamics in section 3, followed by a succinct presentation of the origin of that structure in inflationary models in section 4. Sections 5 and 6 are devoted to more observational aspects reviewing what we have learnt from galaxy catalogues and weak lensing catalogues. Finally the last section is devoted to the new challenges observational cosmology has had to cope with.

2. Dark matter in astrophysical objects

The fact that a significant amount of invisible matter might exist in the universe dates back to the early investigations of Zwicky [108] in the early 1930s on the mass content of galaxy clusters. He pointed out that the velocity dispersion of galaxies within clusters provides an estimate of the amount of matter required to account for the depth of the cluster potential wells. To his own surprise he found that the galaxy cluster mass estimated in such a way exceeds by far the visible mass, that is, the mass of the stars in the cluster galaxies. Such observations have been repeated many times over the last decades using different strategies to trace the amount of mass within large astrophysical objects such as galaxy clusters.

2.1. Mass content in gravitationally bound objects

There are roughly two different strategies to gain access to the amount of mass in cosmological structures. One is through the observation of velocity dispersion of objects within the potential well of the structure, these objects being either galaxies, the line-of-sight velocities of which are measurable using their redshifts, or gas, whose temperature can be obtained from its bremsstrahlung emission. The other method for obtaining the constraints on the amount of matter in cosmological structures is by using gravitational lens effects.

The mass estimates from velocity dispersion rely on some simple, but sometimes questionable, assumptions on the dynamical state of the object. In particular, it is assumed that the object has reached an equilibrium state so that the virial theorem can be applied. Indeed, assuming that the inertial moments of the object are no longer evolving, it is possible to directly relate the internal velocity dispersion of the object to its mass distribution. More specifically, this relation reads,

$$\frac{1}{2}\sum_{ij}\frac{Gm_im_j}{|\boldsymbol{r}_i-\boldsymbol{r}_j|}=\frac{\mathrm{d}^2\sum_i m_i\boldsymbol{r}_i^2/2}{\mathrm{d}t^2}-\sum_i m_i\left(\frac{\mathrm{d}\boldsymbol{r}_i}{\mathrm{d}t}\right)^2, \tag{1}$$

where the term on the left-hand side is the potential energy U, the first term on the right-hand side is the time derivative of the inertial moment of the masses and the second is twice the kinetic energy $K=(1/2)\sum_i m_i v_i^2$. At equilibrium we, therefore, have $U=-2K$ which, for a given profile, provides a relation between the velocity dispersion and the depth of the potential, that is, its mass.

This relation was the basis for the earliest studies of the bound mass of galaxies or galaxy clusters. Zwicky [108], for instance, determined galaxy cluster mass from the measurement of the galactic velocity dispersion. As mentioned earlier, it was the first evidence pointing to the existence of a dark matter component. The x-ray observations of galaxy clusters have confirmed the observations made from the galaxies for the estimated depth of the galaxy cluster potentials. With a new generation of satellites such as Chandra [111] and XMM-Newton [112] it is now possible to get detailed maps of the x-ray emission areas of galaxy clusters.

Those analyses, however, suffer from intrinsic limitations because they are based on certain assumptions on the physical properties of the objects. This is not the case for lens effect observations that are described in the following sections.

2.2. A probe of gravitational potentials: gravitational lenses

The use of gravitational lenses to probe the large-scale structure of the universe is a rather recent and promising approach.

2.2.1. Geometric optics in cosmology. Gravitational lens effects are well-known consequences of general relativity: any mass concentration is going to deflect photons that are passing by with a fraction angle per unit length, $\delta\theta/\delta s$, given by

$$\frac{\delta\boldsymbol{\theta}}{\delta s} = -2\frac{\boldsymbol{\nabla}_{\boldsymbol{x}_\perp}\Phi}{c^2}, \tag{2}$$

where the spatial derivative is taken in a plane perpendicular to the photon trajectory and Φ is the gravitational potential.

It is to be noted that in any practical situation, the total deflection angle is at most a fraction of an arcmin. This is, in particular, the case for the most massive galaxy clusters. It implies that in practice it is possible to ignore the bending of the trajectories in the computation of the lens effects. This is the Born approximation.

One can make another approximation by noting that in general the deflection takes place along a very small fraction of the trajectory between the sources and the observer. One can then assume that the lens effect is instantaneous and is produced through the crossing of a thin plane, the lens plane. This is the thin lens approximation.

2.2.2. The induced displacement. The direct consequence of this bending is a displacement of the apparent position of the background objects. This apparent displacement depends on the distance of the source plane, D_{OS}, and on the distance between the lens plane and the source plane D_{LS}. More precisely, we have

$$\boldsymbol{\beta} = \boldsymbol{\alpha} - \frac{2}{c^2}\frac{D_{\mathrm{LS}}}{D_{\mathrm{OS}}D_{\mathrm{OL}}}\boldsymbol{\nabla}_\alpha\left(\int \mathrm{d}s\ \Phi(s,\alpha)\right). \tag{3}$$

where $\boldsymbol{\alpha}$ is the position in the image plane, $\boldsymbol{\beta}$ is the position in the source plane. The gradient is taken here with respect to the angular position (this is why a D_{OL} factor appears). The total deflection is obtained by an integration along the line-of-sight (a computation usually done assuming the lens is thin). Note that in a cosmological context the general expression for the angular distances are background dependent.

2.2.3. The amplification matrix. Actually, the image of a background object is not only displaced, it is also deformed. This effect is due to variations of the displacement field with respect to the apparent position. These variations induce a change of both the size and shape of the background objects. To quantify this effect one can compute the amplification matrix $\mathcal{A}$, which describes the linear change between the source plane and the image plane:

$$\mathcal{A} = \left(\frac{\partial\alpha_i}{\partial\beta_j}\right). \tag{4}$$

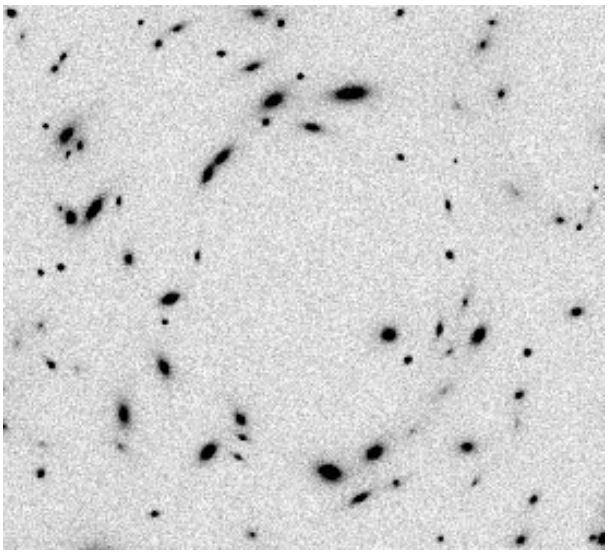

Figure 1. Example of a lens effect on background galaxies on a synthetic image (the lens has no visible counterpart). Both depletion and deformation effects are clearly visible.

Its inverse, $\mathcal{A}^{-1}$, is actually directly calculable in terms of the gravitational potential. It is given by the derivatives of the displacement with respect to the apparent position:

$$\mathcal{A}^{-1} \equiv \frac{\partial \beta_i}{\partial \alpha_j} = \delta_{ij} - 2\frac{D_{\rm LS}}{D_{\rm OS} D_{\rm OL}}\phi_{,ij}, \tag{5}$$

where ϕ is the projected potential,

$$\phi(\alpha) = \int \mathrm{d}s\, \Phi(s, \alpha). \tag{6}$$

This matrix encodes the deformation and amplification that affect images of background objects. Critical lines, which are lines on the image plane where the determinant of $\mathcal{A}^{-1}$ vanishes, can be visualized with giant arcs if a background galaxy happens to intersect its light cone (see figure 1). Such a situation is frequently encountered towards galaxy clusters.

2.3. Galaxy clusters as gravitational lenses

The study of lens galaxy clusters has become a very active field since the discovery of the first gravitational arc by Soucail and collaborators [92] in the Abell cluster A370. The magnitude of the lens effects is directly dependent on the mass distribution within the lens. With detailed observations such as those obtained with the HST it is possible to do a non-parametric reconstruction of the cluster gravitational potential. The strong lensing regime (i.e. the regime corresponding to systems of giant arcs and multiple images) probes the mass distribution of clusters at a scale of about $100\,\mathrm{h}^{-1}$ kpc. To illustrate how lens effects are related to the cluster internal properties it is interesting to approximate the mass distribution of galaxy clusters with isothermal profiles, $\rho_{\rm cluster}(r) \sim r^{-2}$. In this case, when expressed in terms of its internal velocity dispersion, the projected potential of the cluster reads,

$$\varphi(r) = 2\pi\sigma^2 r. \tag{7}$$

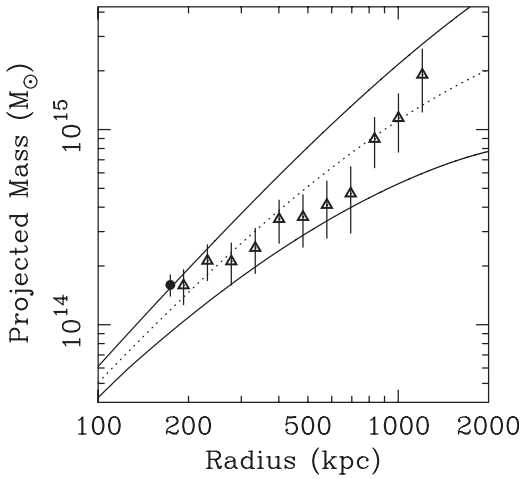

Figure 2. A comparison of the projected total mass determined from the Chandra x-ray data [3] with the strong lensing result [84] (●) and weak lensing results [94] (△). The best-fit NFW x-ray mass model is shown as (· · · · · ·), with 68% confidence contour levels as (——).

As a consequence, the amplification matrix reads,

$$\mathcal{A}^{-1} = \begin{pmatrix} 1 & 0 \\ 0 & 1 - \frac{R_{\rm E}}{r} \end{pmatrix}, \tag{8}$$

where $R_{\rm E}$ is the *Einstein radius*,

$$R_{\rm E} = \frac{4\pi}{c^2} \frac{D_{\rm LS}}{D_{\rm OS}} \sigma^2, \tag{9}$$

so that in this case there is a single critical line that forms an Einstein ring at an angular distance $R_{\rm E}$ from the cluster centre. If the lens–source distances are known, such an observation provides a method of determining the cluster velocity dispersion.

Lensing observations have shown that such approaches, finally, lead to comparable estimates of the mass content of galaxy clusters. This is illustrated in figure 2 from Allen *et al* [3], which shows the mass profile of the Abell 2390 cluster either from Chandra x-ray observations or from lensing constraints (e.g. strong lensing effects with the position of giant arcs and weak lensing observations). What is apparent from this figure is that, despite different physical assumptions, these two approaches provide a coherent picture. With such an observed mass in the galaxy cluster, the mass to light ratio is about 1000 times larger than the solar mass to light ratio. For such a difference to be explained it is not enough if a large fraction of the baryons remain dark (i.e. are not in stars, the average star mass to light ratio being about three times the solar one) but it is also necessary that the matter density of the universe is much greater than the one of baryons given by nucleosynthesis computations. This calls again for a dark matter component that can be clustered, but has weak if any interaction with baryonic matter and photons.

We can already see that lensing observations can also be useful even for non-critical systems if deformations of a large number of background objects can be detected. It then provides clues on how the projected potential behaves. This is the idea pursued in weak lensing observations. We will come back to such observations later.

Other evidence for the existence of dark matter has come from the observation of the rotation curves of spiral galaxies for which the light distribution can be easily observed. After years of investigation it is clear to all astrophysicists that there are no alternatives but to either

introduce this new matter component or to go for much more dramatic changes— a change in the law of gravity at extra-galactic scales.

2.4. The nature of dark matter

It is well known that, so far, direct searches for dark matter have been unsuccessful. In the context of theories of high-energy physics beyond the standard model, good dark matter candidates are the weakly interacting massive particles (WIMPS) that can be found in supersymmetric extensions of the standard model, in which they identify with the lightest supersymmetric particle (LSP).

Such particles are supposed to be relics of the freezing of interacting particles that existed when the universe was at a higher temperature. The present day number density and mass fraction of those particles is a result of the temperature decrease of the universe during its expansion, which causes a rapid decay of the particle cross-sections.

Another possible candidate for dark matter is the axion. These particles have been introduced to account for the fact that strong interactions preserve P and CP symmetries whereas weak interactions do not. The solution Perccei and Quinn have introduced [81] to solve this CP non-violation issue involves the appearance of a light boson Goldstone particle, the axion. That it is a low mass particle should not be seen as an issue. Axions might have been produced in non-thermal processes in the early universe so that nothing prevents them from being non-relativistic particles at the horizon crossing time [65].

The direct search for these particles depends on the nature of their putative interaction with ordinary matter. The current best constraints are provided by the Edelweiss experiment, see figure 3, which aims at detecting WIMP type dark matter particles. The exclusion domain is shown as a red (thick, dark grey) solid line. Domains corresponding to supersymmetric models are shown as dashed black and green (thick, light grey) solid lines. Some models are already excluded, although the bulk of these models lie in an area that is still beyond experimental sensitivity. Other possible strategies for detecting dark matter particles are less direct. They

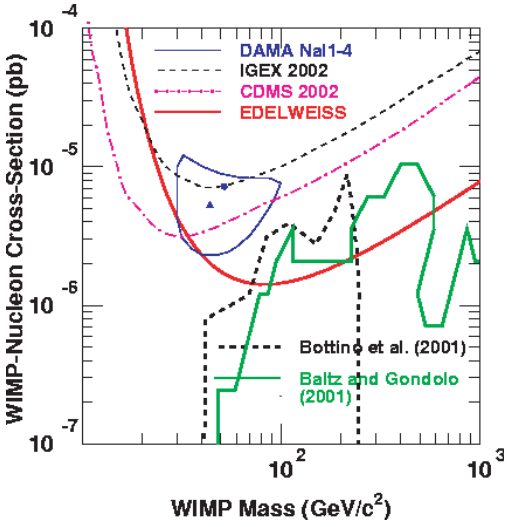

Figure 3. Exclusion zone provided by the Edelweiss experiment for the WIMP cross-section as a function of their mass, from [10].

rely on the detection of the secondary relics, which could be neutrinos or high energy cosmic rays, of dark matter particles when they annihilate in the core of dense objects such as the sun or the galaxy centre. Attempts to detect the signature of such an effect have been unsuccessful so far.

Although direct searches for dark matter have failed so far, their existence is needed, not only to account for the mass content of large astrophysical objects but also as the essential ingredient for the understanding of the observed large-scale matter clustering properties.

3. The growth of structure

3.1. The observed density fluctuation power spectrum

Important constraints can be gathered from the large-scale structure of the universe at the present day and the evolution of the statistical properties of the matter distribution in the local universe. The local density field is denoted in this review by $\rho(\boldsymbol{x})$. The aim of such studies is to understand how the statistical properties of the local density fluctuations, $\delta(\boldsymbol{x}) \equiv \rho(\boldsymbol{x})/\bar{\rho} - 1$ are shaped by the matter and energy content of the universe. The field $\delta(\boldsymbol{x})$, viewed as a classical stochastic field, is conveniently described in terms of Fourier modes:

$$\delta(\boldsymbol{x}) = \int \frac{\mathrm{d}^3\boldsymbol{k}}{(2\pi)^3} \delta_{\boldsymbol{k}}\, \mathrm{e}^{\mathrm{i}\boldsymbol{k}\cdot\boldsymbol{x}}. \tag{10}$$

For a statistically isotropic and homogeneous universe the modes $\delta_{\boldsymbol{k}}$ have a vanishing cross-correlation for different values of the wave vector $\boldsymbol{k}$ and the amplitude of the auto-correlation function does not depend on the direction of $\boldsymbol{k}$. More precisely, one can define the power spectrum $P(k)$ as,

$$\langle \delta(\boldsymbol{k})\delta(\boldsymbol{k}')\rangle = \delta_{\mathrm{Dirac}}(\boldsymbol{k}+\boldsymbol{k}')P(k). \tag{11}$$

The measure of the amplitude and shape of $P(k)$ is one of the major goals of modern cosmology. It traces both the physical context during which the gravitational instabilities developed and the mechanisms that originally gave birth to the density fluctuations. The latter are rather speculative but the most widely accepted one takes place in scenarios of inflation [47,76]. This mechanism and its consequences will be described in some detail at the end of this section. In inflationary scenarios a scalar quantum field, the inflaton, is responsible for an inflationary phase, during which the expansion rate is accelerated, so that the horizon, at the comoving scale, is rapidly shrinking. The quantum fluctuations of the inflaton field can then serve as seeds of the large-scale structure.

The mechanism is roughly the following: during the inflationary phase the wavelength of these fluctuations rapidly exceeds the size of the horizon which, as a result, freezes the inflaton fluctuations in metric perturbations. It is only at later time, during standard expansion phases, when the horizon size becomes large enough again to encompass these metric fluctuations, that gravitational and non-gravitational interactions can play a role. At decoupling, that is, on the last scattering surface, waves of very small amplitudes are imprinted on the density field of the dark matter component. These metric fluctuations will become the large-scale structures of the universe amplified by gravitational instabilities.

Figures 4 and 5 show the clustering properties of the galaxies as they can be observed in the current large-scale galaxy catalogues. The first plot shows the two-point density contrast correlation function as measured in a galaxy angular catalogue. In this case it is assumed that the local number density of galaxies represents the projected density contrast. What is measured is then the two-point angular correlation function, $w_2(\theta)$, of the galaxy number density field, that is the excess probability of finding a galaxy at a finite angular distance θ from

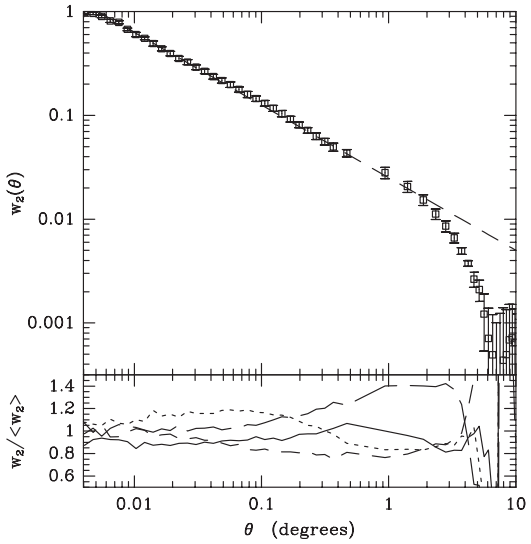

Figure 4. The two-point angular correlation function $w_2(\theta)$ (squares with error-bars), estimated from counts-in-cells and pair-counts in the APM map compared with a power-law $w_2 \sim \theta^{-0.7}$ (- - - -). Errors are from the dispersion in four disjoint subsamples within the APM. The lower panel shows the ratio of the values in each zone to the average value in the whole sample.

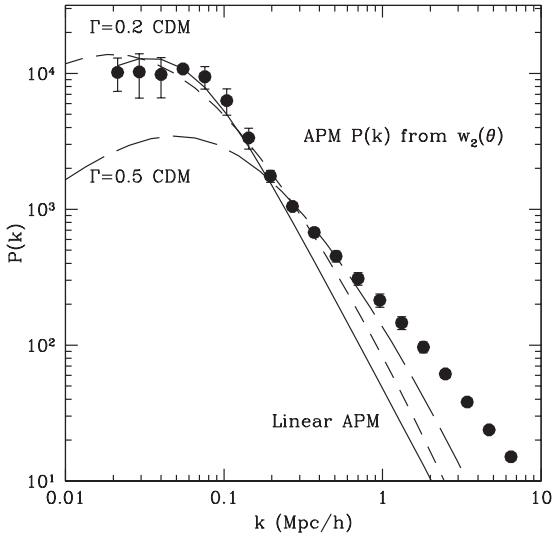

Figure 5. The APM three-dimensional power spectrum reconstructed from $w_2(\theta)$ ($\cdots\cdots$). The continuous line shows a linear $P(k)$ reconstruction. The short and long dashed lines show linear CDM models with $\Gamma = 0.2$ and 0.5, normalized to the data at $k \simeq 0.3\,\mathrm{h\,Mpc^{-1}}$. The behaviour at large k, $k > 0.4$ (that is, at small scale), in the data points is thought to be due to the non-linear dynamical effects that are not taken into account in the theoretical predictions.

a given one. More precisely if n_g is the number density of galaxies, $n_g \mathrm{d}^2\alpha$ is the probability of finding one galaxy within an infinitesimal area $\mathrm{d}^2\alpha$ taken at random in the survey and if this area lies at distance θ from any given galaxy of the survey this probability is changed to $n_g(1 + w_2(\theta))\mathrm{d}^2\alpha$.

As can be observed in figure 4, the galaxy angular two-point correlation has been measured with exquisite precision over the last few decades. Assuming that the large-scale galaxy distribution can be viewed as a mere Poisson realization of the underlying continuous matter, it is then possible to reconstruct the real space three-dimensional power spectrum as defined in equation (11) [43]. This is presented in figure 5. This figure shows the state of the art for our knowledge of the large-scale galaxy clustering properties in the universe. This plot is compared to the prediction of several models. All of them are CDM like. As will be described in the following, this observation can be accounted for by simple gravitational instabilities only if those instabilities are supported by a large amount of non-relativistic dark matter present in the cosmic fluid.

3.2. The motion equation of non-relativistic particles in an expanding universe

Although the nature of dark matter has not yet been identified, candidates for CDM particles are extremely light compared to the mass scale of typical galaxies (except for dark matter fluid, which is in fact a boson condensate, in which case the dynamical evolution obeys specific rules). The expected number density of particles is at least 10^{50} particles per Mpc^3 [65]. In this limit, where the number of particles is large, discreteness effects such as two-body relaxation are negligible (which are, however, important in objects like globular clusters), and collisionless dark matter[1] obeys the Vlasov equation for the distribution function in phase space (equation (22)). This is the master equation from which all subsequent calculations of gravitational instability are derived.

Since baryons or CDM particles are non-relativistic, at scales much smaller than the Hubble radius the equations of motion reduce essentially to those of Newtonian gravity. The expansion of the universe simply calls for a redefinition of the variable used to describe the position and momentum of particles, and a redefinition of the gravitational potential.

Let us therefore consider a set of particles of a mass m that interact only gravitationally in an expanding universe. The equation of motion for a particle of velocity $\boldsymbol{v}$ at position $\boldsymbol{r}$ is thus,

$$\frac{\mathrm{d}\boldsymbol{v}}{\mathrm{d}t} = Gm \sum_i \frac{\boldsymbol{r}_i - \boldsymbol{r}}{|\boldsymbol{r}_i - \boldsymbol{r}|^3}, \tag{12}$$

where the summation is made over all other particles at position r_i.

In the limit of a large number of particles, this equation can be rewritten in terms of a smooth gravitational potential due to the particle distribution,

$$\frac{\mathrm{d}\boldsymbol{v}}{\mathrm{d}t} = -\frac{\partial \phi}{\partial \boldsymbol{r}}, \tag{13}$$

where ϕ is the Newtonian potential induced by the local mass density $\rho(\boldsymbol{r})$,

$$\phi(\boldsymbol{r}) = G \int \mathrm{d}^3\boldsymbol{r}' \frac{\rho(\boldsymbol{r}')}{|\boldsymbol{r}' - \boldsymbol{r}|}. \tag{14}$$

In the context of gravitational instabilities in an expanding universe we have to consider the departures from the homogeneous Hubble expansion. Positions of particles are described by their comoving coordinates $\boldsymbol{x}$ such that the physical coordinates are $\boldsymbol{r} = a(t)\boldsymbol{x}$ where a is the cosmological scale factor so that particles that are at rest in the expanding universe have a fixed $\boldsymbol{x}$. The equations of motion that follow derive from equation (13). They are valid in

[1] There has recently been a renewed interest in studying collisional dark matter [93, 106, 30], which may help solve some problems with collisionless CDM at small scales, of the order of a few kpc.

an arbitrary homogeneous and isotropic background universe. The latter evolves according to the Friedmann equation,

$$\left(\frac{\dot{a}}{a}\right)^2 = H^2 = \frac{8\pi G}{3}\rho_{\rm tot} - \frac{k}{a^2}, \tag{15}$$

where H is the Hubble constant and $k = -1, 0, 1$ depending on the spatial curvature. This equation drives the expansion rate of the universe. Here, the total energy density of the universe, $\rho_{\rm tot}$ includes a possible cosmological constant. This equation is often rewritten in terms of reduced variables,

$$1 = \Omega_{\rm tot} + \Omega_{\rm k}, \tag{16}$$

where $\Omega_{\rm tot} = \rho_{\rm tot}(t)/\rho_{\rm crit}(t)$, $\rho_{\rm crit}$ being the critical density of the universe, e.g. $\rho_{\rm crit} = 3H^2/(8\pi G)$. Similarly, one can define $\Omega_{\rm m}$ as the ratio of matter density to critical density, Ω_Λ as the ratio of vacuum energy density to the critical density and $\Omega_{\rm k} = -k/(H^2a^2)$. Note that $\Omega_{\rm m}$ and Ω_Λ are time dependent.

The peculiar velocity $\boldsymbol{u}$ is defined as

$$\boldsymbol{v}(\boldsymbol{x}, t) \equiv H\boldsymbol{r} + \boldsymbol{u}(\boldsymbol{x}, t), \tag{17}$$

and the cosmological gravitational potential Φ with

$$\phi(\boldsymbol{x}, t) \equiv -\frac{1}{2}\frac{\ddot{a}}{a}\, r^2 + \Phi(\boldsymbol{x}, t), \tag{18}$$

so that the latter is sourced only by density fluctuations, as expected; indeed the Poisson equation reads,

$$\nabla^2\Phi(\boldsymbol{x}, t) = 4\pi G a^2\bar{\rho}\delta(\boldsymbol{x}, t) = \tfrac{3}{2}\Omega_{\rm m}(t)H^2(t)a^2\delta(\boldsymbol{x}, t). \tag{19}$$

In the following we will only use comoving coordinates as the spatial variable so that all space derivatives should be understood as being done with respect to $\boldsymbol{x}$.

The equation of motion, equation (13), then reads

$$\frac{{\rm d}\boldsymbol{p}}{{\rm d}t} = -m\nabla\Phi(\boldsymbol{x}), \tag{20}$$

with

$$\boldsymbol{p} = am\boldsymbol{u}. \tag{21}$$

Let us now define the particle number density in phase space by $f(\boldsymbol{x}, \boldsymbol{p}, t)$; phase space conservation implies the Vlasov equation,

$$\frac{{\rm d}f}{{\rm d}t} = \frac{\partial f}{\partial t} + \frac{\boldsymbol{p}}{ma^2}\cdot\nabla f - m\nabla\Phi\cdot\frac{\partial f}{\partial \boldsymbol{p}} = 0. \tag{22}$$

As it stands, this equation is very difficult to solve, being a non-linear partial differential equation involving seven variables. The non-linearity is included in the dependence of Φ on the integral of the distribution function over momentum, through the Poisson equation. To get an insight into the complete system, one needs to rely on complicated numerical simulations. In most of these simulations the phase space density field is represented by a set of discrete points. Such simulations were first developed in the mid-1980s [31]. They considerably helped our understanding of gravitational instabilities and the formation of the first structures.

In the early stage of the evolution it is, however, possible to gain an insight into the behaviour of the density field by means of simple analytical investigations. This is based on a number of simple approximations. First of all, after matter decoupling, the matter fluid, thought to be composed of baryonic matter and a cold dark matter component, is precisely cold,

in the sense that its intrinsic, thermal, velocity dispersion is much lower that the large-scale flow that the gravitational instabilities can generate. Or, in other words, the pressure forces that are exerted on the matter fluid due to non-gravitational interactions within the matter fluid, or with radiation, are negligible compared to the gravitational forces. Then, large cosmic velocity dispersion will be re-generated during the process of structure formation only within massive astrophysical objects such as galaxies or galaxy clusters. However, to analyse the growth of the density perturbation in the large-scale wiggles it is possible to assume that at each location in space all particles have acquired the same peculiar velocity. At those stages the function f can then be written as,

$$f(\boldsymbol{x},\boldsymbol{p},t)\,\mathrm{d}^3\boldsymbol{x}\,\mathrm{d}^3\boldsymbol{p} = \rho(\boldsymbol{x})\delta_{\mathrm{Dirac}}\left[\boldsymbol{p} - am\boldsymbol{u}(\boldsymbol{x})\right]\,\mathrm{d}^3\boldsymbol{x}\,\mathrm{d}^3\boldsymbol{p}, \tag{23}$$

where $\boldsymbol{u}(\boldsymbol{x})$ represents the local cosmic velocity field. Within this assumption the equation of motion can be replaced by a set of non-linear field equations,

$$\frac{\partial}{\partial t}\delta + \nabla[(1+\delta)\boldsymbol{u}] = 0, \tag{24}$$

$$\frac{\partial \boldsymbol{u}_i}{\partial t} + \frac{\dot{a}}{a}\boldsymbol{u}_i + \frac{1}{a}(\boldsymbol{u}_j.\nabla_j)\boldsymbol{u}_i = -\frac{1}{a}\nabla_i\Phi, \tag{25}$$

which form a closed set with the Poisson equation. This system is still non-linear and necessitates further approximations. This can be done by noting that in the early stages of structure growth the density contrasts are small, much less than unity, which permits the linearization of this system. The resulting cornerstone equation for the linear growth rate of the perturbation is obtained by eliminating the velocity divergence in these two equations and using equation (19) which reads,

$$\frac{\partial^2\delta}{\partial t^2} + 2\frac{\dot{a}}{a}\frac{\partial\delta}{\partial t} = 4\pi G\bar{\rho}_{\mathrm{m}}\delta. \tag{26}$$

It is remarkable that the time dependence of the local density contrast of this equation is scale independent. It is given by the growing mode of the equation,

$$\frac{\mathrm{d}^2 D}{\mathrm{d}t^2} + 2\frac{\dot{a}}{a}\frac{\mathrm{d}D}{\mathrm{d}t} = \frac{3}{2}\Omega_{\mathrm{m}}(t)H^2(t)D. \tag{27}$$

Clearly, the growth of structures depends on the matter content of the universe. Note that the right-hand side of the above equation is proportional to Ω_{m}. Then, if the fraction of the cosmic energy density of matter type drops, the growth of the structure is stopped (but the structures survive, they are not washed out).

3.3. Gravitational instabilities: from radiation domination to matter domination

Equation (27) describes the linear growth of structure when the universe is dominated by the matter content. In earlier stages, however, this is not the case. The previous system of equations is then changed in two ways. First, the pressure force plays a role, in particular, for the baryonic matter that can interact with the radiation. Second, the gravitational instabilities can also be sustained not only by the matter density fluctuations but also by the radiation energy fluctuations.

The behaviour of modes will then depend on the epoch at which they enter the horizon (e.g. the time at which the inverse Hubble size reaches their size). Before that epoch the metric fluctuations are simply frozen. For modes of cosmological interest, this happens typically at the recombination time (when electrons and protons recombine to form a transparent medium giving birth to the cosmic microwave background), the equivalence time (when the radiation and matter energy density are equal) or earlier.

The very large-scale modes, those that are larger than the horizon at recombination time, re-enter the horizon when the universe is matter dominated so that pressure is negligible at that time. The gravitational instability can then fully develop according to equation (26).

At smaller scales, for modes that enter the horizon when the universe is radiation dominated, fluctuations in the radiation fluid are damped because of the pressure effects. Formally, in the presence of pressure, equation (26) can be written as

$$\frac{\partial^2\delta}{\partial t^2} + 2\frac{\dot{a}}{a}\frac{\partial\delta}{\partial t} = 4\pi G\bar{\rho}(t)\delta + \frac{1}{a^2}\frac{\delta P}{\delta\rho}\nabla^2\delta. \tag{28}$$

The pressure term prevents instabilities from developing in the fluid, where the pressure is large, that is radiation or baryon fluid before decoupling. What happens to the density fluctuations in the matter fluid strongly depends on the nature of matter in the universe. In particular, the presence of a significant amount of dark matter is crucial to sustain the small-scale matter density fluctuations. Baryons, because they are tightly coupled to the photons, cannot play this role between horizon crossing and recombination. To understand this point it is very illuminating to consider the plot in figure 6. It shows the evolution of the amplitude of the density fluctuation of a rather small-scale vector mode (about $100\,h^{-1}$ kpc).

In this plot, the short-dashed line shows the amplitude of the density fluctuations in the baryon component, compared to the one in the radiation component (long-dashed line) and dark matter component (solid line). One can see that before Hubble size crossing (which takes place for this particular mode at $a/a_0 \approx 3 \times 10^{-6}$), the three components behave alike. After that, baryons and photons are still tightly coupled together and because of the pressure term they enter a regime of acoustic oscillations. The dark matter component decouples from the two others. Its fluctuations are, however, sustained by the baryon-radiation component before equivalence. Till that time the dark matter density fluctuations are frozen (the right-hand side of equation (26) is to be replaced by $4\pi G\bar{\rho}_{\rm rad}\delta_{\rm rad}$, which is damped.) As a result the density fluctuation growth is only logarithmic. It resumes normally after equivalence when the potential is again mainly sourced by the dark matter component. The baryon component joins the dark matter component after decoupling: basically it amounts to saying that the baryons

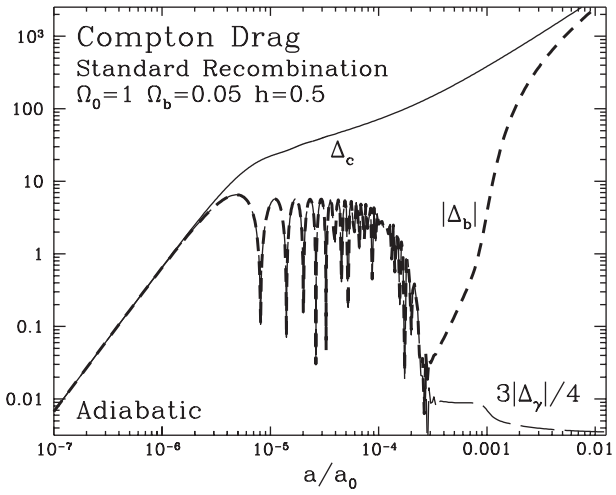

Figure 6. Evolution of the amplitude of a small-scale mode (about $100\,h^{-1}$ kpc) in the different components of the cosmic fluid. The dashed line corresponds to the baryon component and the solid line to the dark matter component; from [53].

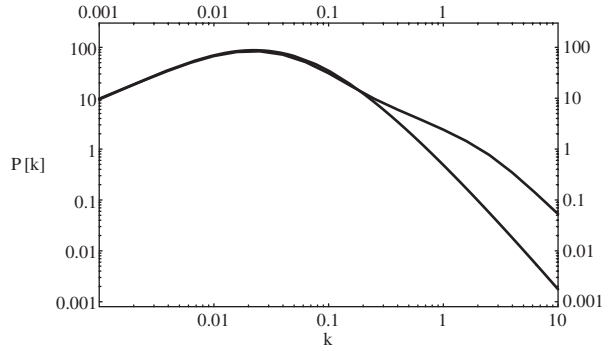

Figure 7. Shape of the matter power spectrum in a log–log plot for a CDM type model. The upper line shows the small-scale non-linear evolution of the power spectrum.

fall into the dark matter potential wells that survived the radiation dominated epoch. Clearly if there were no dark matter component, the amplitudes of the density fluctuation would be dramatically smaller at small scale today.

The fate of the density fluctuations then depends on the fluctuation wavelength: if it is such that horizon crossing takes place after equivalence the instability growth is hardly affected, otherwise they are all the more attenuated, such that the time between horizon crossing and equivalence is large. Then, when the behaviour of modes of different wavelength are considered, we are left with a generic shape for the power spectrum as shown in figure 7. In this picture, we have assumed that the primordial (superhorizon) density fluctuations are given by an Harrison–Zel'dovich spectrum. It is a spectrum where the metric fluctuations are independent of scale. In terms of the matter density power spectrum, it amounts to saying that $P(k) \sim k$ (e.g. a k^4 factor appears due to the Poisson equation). Then, the matter power spectrum is expected to behave as follows:

- at large scale, as a power law behaviour that scales like k;
- at small scale, as a power law behaviour that scales like k^{-3};
- and to exhibit a transition scale, $k_{\rm eq}$, corresponding to the scale that equals the inverse of the horizon size at equivalence. It is about $10\,{\rm h}^{-1}\,{\rm Mpc}$.

The detailed shape of the power spectrum obviously depends on the cosmological parameters. However, it is mainly driven by the value of $k_{\rm eq}$, that is by the value of the parameter,

$$\Gamma = \Omega_0\, h, \tag{29}$$

where h is the value of the Hubble constant in units of $100\,{\rm km\,s^{-1}\,Mpc^{-1}}$. Note that the subsequent non-linear evolution of the density field will affect the shape of the power spectrum at small scale because of mode coupling effects (upper line). This non-linear evolution can be predicted to some extent with the use of Hamilton *et al* 's prescription [51] or one of its extensions like the Peacock and Dodds fitting formulae [80]. What these formulae tell us is that once the linear local density contrast has reached a threshold value its growth is over-amplified. Such effects obviously take place at different times for different scales, so that the final power spectrum shape is determined by the history of the linear growth rate of the fluctuations. The resemblance of this picture to the actual observations is striking, although the size of the current surveys is still too limited for the small k behaviour to be visible in the actual data.

The picture obtained here is undoubtedly attractive because of its rather limited number of ingredients and the robustness of the predictions. It relies again on the assumption that gravitational instabilities are to some extent sustained by a cold dark matter component.

3.4. The cosmic microwave background anisotropies

Another precious window for studying the large-scale structure is the measurement of the CMB temperature anisotropies. Indeed, it represents a direct snapshot of the temperature and metric fluctuations at a well defined time, the recombination time, or, in terms of a more geometrical point of view, on the last scattering surface.

There are two reasons for such a probe to be so attractive: first, what is observed can be directly related to the cosmic fluid behaviour and, second, the physical mechanisms that are involved are well within the linear regime. CMB temperature fluctuations are therefore a direct window on the mechanisms at play for the formation and evolution of the large-scale inhomogeneities. It is, however, beyond the scope of this paper to detail all the physical processes that shape the CMB temperature power spectrum. It is, nonetheless, possible to grasp the essentials of it through simple arguments.

Let us denote by θ the local temperature fluctuations on the last scattering surface. The observed temperature on the last scattering surface is then the superposition of the intrinsic local temperature fluctuations and the local gravitational potential ϕ (due to gravitational Doppler effects) and the Doppler effects caused by the plasma motion along the line-of-sight.

- At angular scales larger than the angular size of the Hubble length at the moment of recombination, the observed temperature fluctuations are due to either intrinsic fluctuations or gravitational Doppler effects. The combination of the two is actually proportional to the value of the gravitational potential on the last scattering surface. This is, for instance, what the COBE satellite reported in 1992 [91].
- At scales that are smaller than the horizon, the modes in the radiation fluid had time to enter a regime of acoustic oscillations (as depicted in figure 6). Then, all effects—intrinsic temperature fluctuations, gravitational and motion Doppler effects—play a comparable role.

Similarly to the matter density field, the statistical properties of the temperature anisotropies are usually described through their power spectrum. In this case it is defined from the spherical harmonic decomposition of the temperature of the sky,

$$\frac{\delta T}{T}(\alpha, \beta) = \sum_{l,m} a_{lm} Y^l_m(\alpha, \beta), \tag{30}$$

(α and β are spherical coordinates on the celestial sphere).

From a theoretical point of view the a_{lm} are random variables. Their correlation properties define the temperature power spectrum,

$$\langle a_{lm} a^*_{l'm'} \rangle = \delta^K_{ll'} \delta^K_{mm'} C_l, \tag{31}$$

where δ^K is the Kronecker delta symbol.

In figure 8 are shown examples of theoretical curves of C_l for a few different cosmological models. Note that the scales are logarithmic. One can observe the following properties,

- At large angular scales (small l) one observes a flat plateau corresponding to the Sachs–Wolfe effect. For an initial Harrison–Zel'dovich spectrum, $l(l+1)C_l$ is indeed flat in this regime.
- At intermediary scales, oscillations develop that correspond to the appearance of acoustic oscillations in the plasma below the horizon scale. An aside, but an important one, is that the angular scale at which the first acoustic peak lies corresponds precisely to the angular scale of the sound horizon at the decoupling time. Knowing the physical scale at which it takes place, it provides important information of the overall spatial curvature of the universe. One can also note that the odd and even number peaks do not reach the same

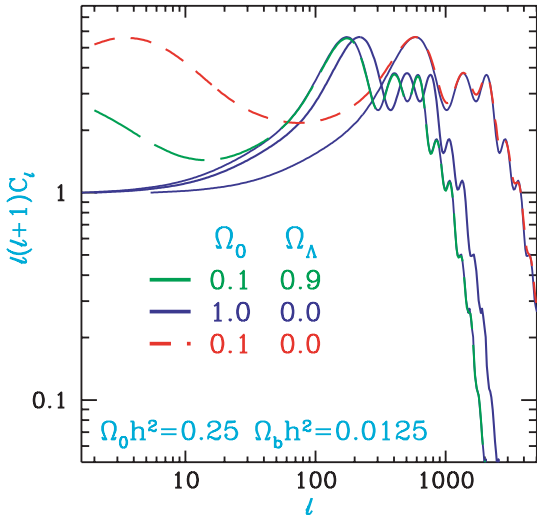

Figure 8. Examples of C_l predictions for CDM type models and for various cosmological parameters, from [53].

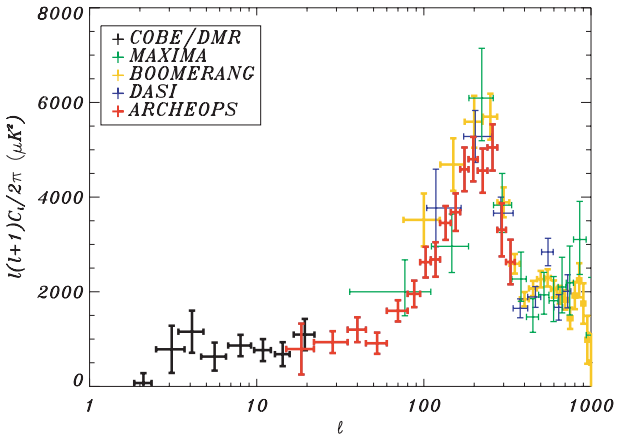

Figure 9. Experimental situation as it was during fall 2002; from [8] that compares COBE, Archeops, Boomerang, Dasi and Maxima results [98, 78, 66, 50].

height. The reason is due to the fraction of baryons coupled to the radiation in the plasma fluid. In the oscillatory motion of the plasma, baryons contribute to the attractive force, because of their mass, but not to the repulsive force, that is, to the pressure. It induces a shift of the zero value of the oscillations, which results in these differences.

- At small scales the angular extension of the density perturbations is similar to the width of the last scattering surface. The image of such a perturbation is then blurred. It translates into an exponential cut-off in the power spectrum.

The observational situation for the C_l is rapidly evolving. In figure 9 data from various experiments completed in fall 2002 are collected . Although the measurement of the C_l spectrum has not yet been done with minute accuracy, the data clearly sketch a curve that resembles the theoretical expectations showing the large-scale Sachs–Wolfe plateau, a few acoustic peaks and the drop in the amplitude at small scales.

The comparison between theoretical models and such observations gives precious insights of varied nature. The mere existence of peaks shows that the fluctuations have the same time phase. This indicates that the metric fluctuations had been imprinted at a much earlier time. More precisely one can gather from observations that

- the position of the first acoustic peak shows that the spatial section of the universe is flat;
- the relative height of the peaks points to a value of a baryonic density in agreement with the primordial nucleosynthesis calculations.

To be more precise, an analysis of the most recent Archeops data in combination with previous CMB data sets [9] constrains the baryon content of the universe to be $\Omega_b h^2 = 0.022(+0.003, -0.004)$, compatible with Big Bang nucleosynthesis and observation of the primordial deuterium abundance and with a similar accuracy. Using cosmological priors obtained from recent non-CMB data leads to yet tighter constraints on the total density, e.g. $\Omega_{\rm tot} = 1.00(+0.03, -0.02)$ using the HST determination of the Hubble constant. The spectral index n of the primordial fluctuations is measured to be $0.96(+0.03, -0.04)$ when the optical depth to re-ionization is fixed to zero.

However, the CMB anisotropies are not necessarily a very good probe of either the dark matter or dark energy content of the universe. The soundest evidence for dark matter, as far as large-scale structure is concerned, is obtained from the comparison of the amplitude of the metric fluctuations on the last scattering surface to that of the local density fluctuations. Such a comparison is presented in figure 10 with recent data sets. It shows a remarkable match between the amplitude of the CMB anisotropies and the density perturbations if and only if the amount of dark matter represents about 30% of the critical density. To be more precise the 2dF Redshift galaxy Survey data (circles) imposes the condition $\Omega_{\rm matter} h = 0.20 \pm 0.03$ [79].

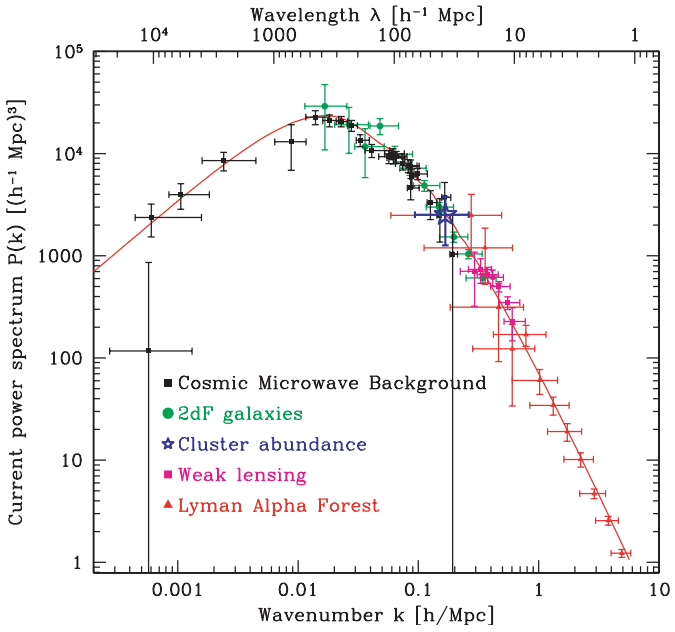

Figure 10. Shape of the matter power spectrum obtained from different types of observations, galaxy catalogues, cluster number density, cosmic shear and Lyman alpha clouds, compared to the predicted shape and amplitude of the power spectrum inferred from CMB observation assuming a Λ-CDM cosmological model; from [99].

4. Origin of structure

The remarkable agreement between the theoretical prediction for the temperature anisotropy power spectrum and observations calls for a mechanism that would be at the origin of the metric fluctuations. Over the last few years, inflation has been the only working scenario. It is beyond the scope of this review to describe inflationary models in much detail. Instead, we refer the reader to recent reviews for a complete discussion [67–69].

4.1. Inflation: motivations and basic principles

The inflationary paradigm cannot yet be viewed as a mature theory. It is, however, undoubtedly a very seductive scenario. Indeed, it gives a number of convincing explanations for different issues that modern cosmology is facing. Its major interest is probably to place a general problem, the initial conditions, within physical investigations. Among the problems it solves are the following:

- The flatness problem—with normal matter, the equation of state of a flat spatial metric corresponds to an unstable region.
- The horizon problem—different parts of the last scattering surface separated by more than 2° have never been in causal contact in standard cosmology. There is thus no possible mechanism that could have set their temperature equal to a precision of 10^{-5}.
- The absence of monopoles—in grand unified theories magnetic monopoles should have formed in large numbers when the universe was hotter but none have been observed.
- Seeds of large-scale structure have also to be found at scales larger than the current Hubble size.

4.2. The 'slow-roll' inflation

The inflationary scenario is based on the physics of a quantum scalar field in an expanding universe. For such a simple field the Lagrangian density reads (for a minimally coupled scalar field) as follows:

$$\mathcal{L}_\varphi = \tfrac{1}{2}\left(\partial_\mu\varphi\partial^\mu\varphi\right) - V(\varphi). \tag{32}$$

This contribution is to be added to the curvature term to obtain the complete Einstein equations of motion. In the following the gravitational constant G will be denoted by

$$G \equiv \frac{1}{m_{\rm pl}^2}, \tag{33}$$

following the notation of high-energy physics.

The dynamical evolution of the field φ is related to that of the expansion factor. In general, the equation of motion of the field φ corresponds to a slight extension of the usual Klein–Gordon equations:

$$\ddot{\varphi} + 3\frac{\dot{a}}{a}\dot{\varphi} - \frac{1}{a^2}\Delta\varphi = -\frac{\mathrm{d}V}{\mathrm{d}\varphi}. \tag{34}$$

The evolution equation of the expansion factor is obtained through the Einstein equations. For a scalar field the local energy density is simply,

$$\rho(\boldsymbol{x}) = \frac{\dot{\varphi}^2}{2} + \frac{(\nabla\varphi)^2}{2} + V(\varphi), \tag{35}$$

so that,

$$\dot{a}^2 = \frac{8\pi a^2}{3m_{\rm pl.}^2}\left[\frac{\dot{\varphi}^2}{2} + \frac{(\nabla\varphi)^2}{2} + V(\varphi)\right]. \tag{36}$$

Two aspects of inflation should be considered. The behaviour of the homogeneous part of the field is responsible for the proper inflationary period. Its fluctuations will serve as the seeds of the large-scale structure.

Therefore, the field φ is written as the sum of two terms

$$\varphi(t, \boldsymbol{x}) = \varphi_0(t) + \delta\varphi(t, \boldsymbol{x}) \tag{37}$$

and one assumes that the motion equation derived from 'classical' general relativity applies to φ_0, whereas we will allow ourselves to quantize $\delta\varphi(t, \boldsymbol{x})$. We will also assume that the major part of the energy density is in φ_0, not in its fluctuations [2]. Then the dynamical evolution of φ_0 can be treated independently of its fluctuations.

The motion equation for φ_0 is

$$\ddot{\varphi_0} + 3\frac{\dot{a}}{a}\dot{\varphi_0} = -\frac{{\rm d}V}{{\rm d}\varphi}(\varphi_0), \tag{38}$$

and that for the expansion factor is

$$\dot{a}^2 = \frac{8\pi a^2}{3m_{\rm pl.}^2}\left[\frac{\dot{\varphi_0}^2}{2} + V(\varphi_0)\right]. \tag{39}$$

In the equation of motion of φ_0 one notices the presence of an extra term that acts as a dissipative term during the expansion. The inflationary period corresponds precisely to a period when this term dominates over the first term of the left-hand side of this equation. It corresponds to a stationary regime where the potential energy 'dissipates' in a rapid overall expansion.

$$\dot{a}^2 = \frac{8\pi G a^2}{3}V(\varphi), \tag{40}$$

$$3\frac{\dot{a}}{a}\dot{\varphi_0} = -\frac{{\rm d}V}{{\rm d}\varphi}(\varphi_0). \tag{41}$$

Roughly the potential value is slowing varying so that the Hubble parameter during that period is only slowly varying. The expansion factor then behaves essentially like,

$$a(t) \sim \exp(Ht) \tag{42}$$

with

$$H(t) = \sqrt{\frac{8\pi V}{3m_{\rm pl.}^2}}. \tag{43}$$

The expansion is then clearly super-luminous: more and more materials are escaping the particle horizons (see figure 11). It sets the stage for developing a viable theory of structure formation.

[2] This assumption will break down at the end of the inflationary period. This is the whole problem of the back-reaction issue.

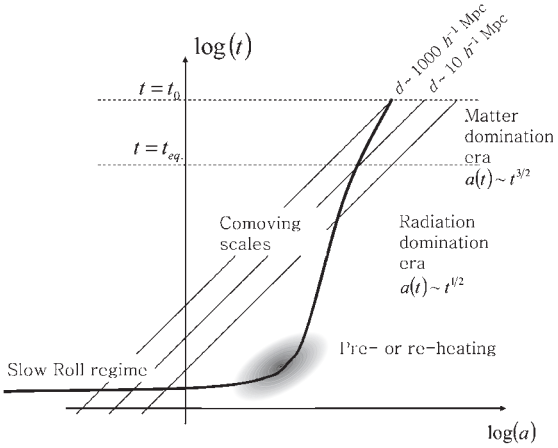

Figure 11. Schematic view of the inflationary scenario showing the time evolution of the expansion factor. It shows that comoving observable scales, that have re-entered the horizon at roughly the equivalence time, actually once escaped the horizon at a much earlier time during the inflationary period.

4.3. The seeds of structures: inflation and quantum fluctuations

In models of inflation the large-scale metric fluctuations originate from fluctuations of the inflaton value in different parts or patches of the now observable universe. Once these patches are super-Hubble their respective histories differ only in the time spent in the inflationary period. As a result, the curvature fluctuations between different parts is simply,

$$\mathcal{R} = \frac{\delta a}{a}. \tag{44}$$

During the inflationary period, and in the slow-roll approximation, the value of $\delta a/a$ is simply given by

$$\mathcal{R} = H\delta t = \frac{3H^2\delta\varphi}{V'(\varphi)}. \tag{45}$$

The metric fluctuations are then simply proportional to the field fluctuations.

The field φ, as any modern, scalar field, should have quantum fluctuations. This fluctuation field can be decomposed in to Fourier modes using the creation and annihilation operators $a_{\boldsymbol{k}}^{\dagger}$ and $a_{\boldsymbol{k}}$ for a given wave mode $\boldsymbol{k}$:

$$\delta\varphi = \int \mathrm{d}^3\boldsymbol{k}\left[a_{\boldsymbol{k}}\psi_k(t)\exp(\mathrm{i}\boldsymbol{k}\cdot\boldsymbol{x}) + a_{\boldsymbol{k}}^{\dagger}\psi_k^*(t)\exp(-\mathrm{i}\boldsymbol{k}\cdot\boldsymbol{x})\right]. \tag{46}$$

The operators obey the standard commutation relation,

$$[a_{\boldsymbol{k}}, a_{-\boldsymbol{k}'}^{\dagger}] = \delta_D(\boldsymbol{k}+\boldsymbol{k}') \tag{47}$$

and the mode functions $\psi_k(t)$ are obtained from the Klein–Gordon equation for φ in an expanding universe. We give, here, its expression for a de-Sitter metric (i.e. when the spatial sections are flat and H is constant):

$$\psi_k(t) = \frac{H}{(2k)^{1/2}k}\left(\mathrm{i} + \frac{k}{aH}\right)\exp\left[\frac{\mathrm{i}k}{aH}\right], \tag{48}$$

where a and H are, respectively, the expansion factor and the Hubble constant that are determined by the overall content of the universe through the Friedmann equations (equations (15) and (16)).

When the modes exit the Hubble radius, $k/(aH) \ll 1$, one can see from equation (48) that the dominant mode reads,

$$\varphi_{\boldsymbol{k}} \approx \frac{\mathrm{i}H}{\sqrt{2}k^{3/2}}\left(a_{\boldsymbol{k}} + a^{\dagger}_{-\boldsymbol{k}}\right), \qquad \delta\varphi = \int \mathrm{d}^3\boldsymbol{k}\varphi_{\boldsymbol{k}}\,\mathrm{e}^{\mathrm{i}\boldsymbol{k}\cdot\boldsymbol{x}}. \tag{49}$$

Thus, these modes are all proportional to $a_{\boldsymbol{k}} + a^{\dagger}_{-\boldsymbol{k}}$. One important consequence of this is that the quantum nature of the fluctuations has disappeared [48, 62, 63]: any combinations of $\varphi_{\boldsymbol{k}}$ commute with each other. The field φ can then be seen as a classical stochastic field where ensemble averages identify with vacuum expectation values,

$$\langle\cdots\rangle \equiv \langle 0|\cdots|0\rangle. \tag{50}$$

After the inflationary phase the modes re-enter the Hubble radius. They leave imprints of their energy fluctuations in the gravitational potential, the statistical properties of which can therefore be deduced from equations (47) and (49). All subsequent stochastic aspects that appear in the cosmic fields can thus be expressed in terms of the random variable $\varphi_{\boldsymbol{k}}$.

One important property of inflationary scenarios is that the primordial fluctuations are expected to obey Gaussian fluctuations. This is a very robust result since the metric fluctuations originate from weak (at 10^{-5} level) fluctuations of a free quantum field. Only in quite elaborate models (with double inflaton fields) is it possible to get some marginal non-Gaussian properties [18].

The primordial seeds are also expected to be adiabatic in the sense that density contrasts in the various cosmic fluids are expected to be proportional to each other.

The other generic result obtained in the inflationary paradigm is less robust, although it emerges in all models based on the so-called 'slow-roll' approximation. In this case indeed the primordial spectrum $P^{\mathrm{prim}}(k)$ indeed closely follows a Harrison–Zel'dovich spectrum,

$$P^{\mathrm{prim}}(k) \sim k. \tag{51}$$

5. Large-scale structure from galaxy catalogues

It is unfortunately not so simple to make use of the galaxy catalogue observations to gain insights into the properties of dark components. What are directly observable are luminous objects, the formation of which is by itself extremely complicated.

5.1. Galaxy cluster number counts

Only in the case of galaxy clusters, which are the most massive gravitationally bound objects to be seen in the sky, is it possible to derive direct constraints on the matter fluctuations. The idea, formulated by Press and Schechter [85], is that such objects form when they have accreted a sufficient amount of matter. The number density of clusters can then be expressed as a constraint on the mass fluctuation amplitude at the mass scale of the clusters. The total mass in galaxy clusters is given by the fraction of matter in the universe that should have been, at a given time, accreted to a cluster whose mass exceeds a given limit, M.

The mass, assumed to be conserved during the collapse of the regions that can give birth to a cluster of mass M, is simply given in terms of R with $M = 4\pi R^3/3$. One should therefore look for the probability that the sphere of radius R encompassing a given point has a density

such that it should now be virialized. This probability then gives the mass fraction in the universe, $f(>M)$, objects of mass larger than M,

$$f(>M) = \int_{\delta_c D_+(t_i)/D_+(t_0)} \mathrm{d}\delta_i \, p(\delta_i, R), \tag{52}$$

where $p(\delta)$ is the probability distribution function of the initial overdensity δ_i for a filtering scale R. For Gaussian initial conditions p is simply a Gaussian distribution of variance $\sigma_i(M)$, depending on the matter density power spectrum and filtering scale.

Then,

$$f(>M) = \frac{1}{2}\left(1 - \mathrm{Erf}\left[\frac{\delta_c D_+(t_i)}{\sqrt{2} D_+(t_0)\sigma_i(M)}\right]\right), \tag{53}$$

so that

$$f(M)\,\mathrm{d}M = \frac{-\delta_c}{\sqrt{2\pi}(D_+(t_0)/D_+(t_i))\sigma_i(M)} \frac{\mathrm{d}\log(\sigma_i(M))}{\mathrm{d}M} \times \exp\left[-\frac{\delta_c^2}{2(D_+(t_0)/D_+(t_i))^2\sigma_i^2(M)}\right] \mathrm{d}M. \tag{54}$$

Using such calculations one can then relate the mass fraction of clusters in a straightforward manner to the statistical properties of the underlying matter field. This is undoubtedly an attractive approach but whose validity is, in many respects, quite questionable. To start with, one can see that the total matter fraction in virialized objects reaches $\frac{1}{2}$, whereas one expects it to be 100% if objects of all masses are taken into account. It so happens that correcting this formula with a mere factor of 2 gives a good account of the results obtained in numerical simulations.

The origin of this discrepancy is that the calculation does not take into account all structures that can possibly accrete a matter point. This point has been clearly illustrated by the analysis of Bond *et al* [23], which provides an alternative interpretation of this formula. Indeed, if one considers top hat filters in k space, then, the search for all structures that can absorb a given point reduces to a random walk problem. With such an approach the factor 2 is automatically recovered, but it nonetheless leaves parts of the general problem unsolved, such as mergers, tidal effects, etc.

However, despite these restrictions, the Press and Schechter theory has been tested to a surprising accuracy against numerical experiments. This is certainly not a complete theory for computing the formation of structures, but as far as rare events are concerned it gives very fruitful insights into the way the number density of galaxy clusters is going to depend on the cosmological parameters.

This theory has been used in particular to infer the amplitude of the mass fluctuations at the cluster mass scale. From the formula (54) it is clear that the cluster number density strongly depends on the amplitude of the mass fluctuations as soon as they correspond to rare events. This is the case for clusters of masses of about $10^{15} M_\odot$. The present constraints are [34],

$$\sigma_8 \Omega_0^{0.55} = 0.5 \pm 0.1, \tag{55}$$

where σ_8 is the density fluctuation at the $8\,\mathrm{h}^{-1}$ Mpc scale, which corresponds roughly to the mass scale of galaxy clusters. The dependence on the value of Ω_0 corresponds partly to the growth rate of the fluctuations, which we know depends on the values of the cosmological parameters and partly on the fact that changing Ω_0 changes the initial radius of the collapsing cluster regions.

This result is extremely important in the sense that it directly probes the amplitude of the mass fluctuations. However, it is somewhat limited because cluster surveys do not yet contain many objects. In principle, it is possible to do better with larger surveys such as galaxy surveys.

5.2. Biasing in galaxy catalogues

The most common way of mapping the large-scale structure of the universe is provided by galaxy catalogues. Assuming that the number density of objects is a somewhat reasonable tracer of the underlying matter density field one can get a picture of the general properties of the mass distribution at large scale. In particular, the shape of the galaxy power spectrum appears to be in agreement with what is expected in CDM type scenarios when normalized on the CMB anisotropy amplitudes [91] (figure 10). This is already an important achievement in defining the growth feature of a valid cosmological model. Testing the details of the model becomes more and more delicate, however, because galaxies cannot be considered as absolutely faithful tracers of the density field, or, in other words, it is very difficult to infer at which level the galaxy catalogues do not give a biased view of the actual large-scale structure of the universe.

To circumvent this problem different strategies have been explored. One is to instead map the large-scale cosmic flows traced by the galaxies. The other is to map the large-scale gravitational potential with lensing observations. These two approaches are reviewed in the following sections.

5.3. Large-scale cosmic flows

The observation of large-scale flows is motivated by the remark that objects embedded in the cosmic fluid are expected to follow the same flow irrespective of their mass. Galaxy peculiar velocities should then account for the total mass fluctuations that surround them. To be more precise, linear theory tells us that the velocity divergence is directly related to the local density,

$$\frac{\nabla \cdot u}{H_0}(\boldsymbol{x}) = -\frac{a}{D_+}\frac{\mathrm{d}D_+}{\mathrm{d}a}\delta(\boldsymbol{x}) \approx -\Omega_0^{0.6}\delta(\boldsymbol{x}), \tag{56}$$

where D_+ is the linear growth rate of the fluctuations and Ω_0 is the present density of the matter density of the universe in units of the critical density. This relation can also be written in an integral form, which simply states that the local flow is proportional to the local gravitational force. As can be seen from equation (56), observations of cosmic flows can give constraints on Ω_0, and such observations have therefore been actively undertaken.

It is, however, a long way from obtaining observational data to the actual construction of velocity surveys. The essential ingredient is given by the Tully–Fisher relation between the absolute luminosity and the internal velocity dispersion of a galaxy. This relation states that

$$L_{\mathrm{abs}} \propto \sigma^4_{\mathrm{galaxy}}. \tag{57}$$

It has been observed and calibrated for cluster galaxies (where all the galaxies are at the same cosmological distance). An apparent luminosity and a measured internal velocity dispersion then give an estimate of the proper distance r of any galaxy. The line-of-sight peculiar velocity is simply obtained from the difference between the redshift distance cz and the Hubble expansion rate $H_0 r$. Finally, it is possible to build the full three-dimensional velocity flows taking advantage of the fact that the large-scale flows are expected to be potential (as long as shell crossings are ignored) [19].

In practice, this method has very strong limitations because the Tully–Fisher relation suffers from a large dispersion, about 15%. The consequences of this dispersion are quite dramatic on the line-of-sight velocities: the statistical error in the determination of the peculiar velocity of a single galaxy reaches 100% at $40\,\mathrm{h}^{-1}$ Mpc. As a consequence, the investigations of the large-scale flows are hampered by several problems:

- large systematic errors (Malmquist bias);
- large 'cosmic variance' due to the small size of the survey.

What we have learnt from the current surveys of large-scale velocity flows remains largely subject to these systematic problems. Early analysis by Dekel and collaborators (see [33]) pointed towards a high value of Ω_0 but the most recent studies are less affirmative (see, for instance, the introductory talk of the 1999 Victoria conference by Strauss [96]) and rather favour values of Ω_0 of the order of 0.3–0.8.

6. Weak lensing measurements

The possibility of actually using lens effects to probe the statistical properties of the large-scale structure as a whole has been investigated in the early 1990s. The difficulty obviously lies in the fact that the distortions induced by the lenses are very small, much smaller than the intrinsic shape fluctuations of the background objects. The projected potential can then only be reconstructed via a statistical analysis of shape measurements of a large amount of background objects.

6.1. Geometric optics in a weakly inhomogeneous universe

What is now the source term for the deflection angle? We should first note that, in the absence of lenses, light rays follow the geodesics of the Friedmann–Robertson–Walker metric, and, in the applications we are interested in, the metric fluctuations are always weak. In general, for a spherically symmetric system, metric fluctuations are given by, $GM/(Rc^2)$. For instance, at the surface of a star of one solar mass (of radius, say, $R = 10^6$ km) it is $\delta\phi \approx 10^{-6}$, at a distance of $R = 1$ Mpc from galaxy clusters of mass $M = 10^{15} M_\odot$ it is $\delta\phi \approx 10^{-5}$. The metric inhomogeneities are thus always extremely weak, for any cosmological situation.

Following Sachs [88], we consider two nearby geodesics, $\mathcal{L}$ and $\mathcal{L}'$, in a light bundle in an FRW universe with small metric fluctuations. We denote by α_i the bi-dimensional angular distance between $\mathcal{L}$ and $\mathcal{L}'$ as it is seen by the observer. This is the distance in the image plane, that is the difference between the angular coordinates at which the photons arrive. We denote $\xi_i(z)$ the real distance between $\mathcal{L}$ and $\mathcal{L}'$ at redshift z (see figure 12). It implies that the geodesics are straight enough so that light always travels towards the observer. We also assume that the deflections are small enough so that it is possible to make the small angle approximation,

$$\xi_i(z) = a\, \mathcal{D}_{ij}(z)\, \alpha_j, \tag{58}$$

that is, we assume the the position vector ξ_i can be obtained by a simple linear transform of the angular coordinates. For a homogeneous space $\mathcal{D}_{ij}(z)$ is simply given by $\mathcal{D}_0(z)\delta^K_{ij}$, where δ^K_{ij} is the Kronecker symbol. Obviously $\mathcal{D}_{ij}$ changes as a function of the redshift along the trajectories. The 'virtual' angular position in the source plane is then given by the ratio of the real distance (at the time of light emission, for instance) to the angular distance of the emitter in a homogeneous space,

$$\boldsymbol{\beta} = \frac{\boldsymbol{\xi}(z)}{a\mathcal{D}_0(z)}. \tag{59}$$

The amplification matrix, or rather its inverse, $\mathcal{A}^{-1}$, is then given by,

$$\mathcal{A}^{-1}(z) = \frac{\mathcal{D}_{ij}(z)}{a\mathcal{D}_0(z)} \tag{60}$$

for a source plane at redshift z.

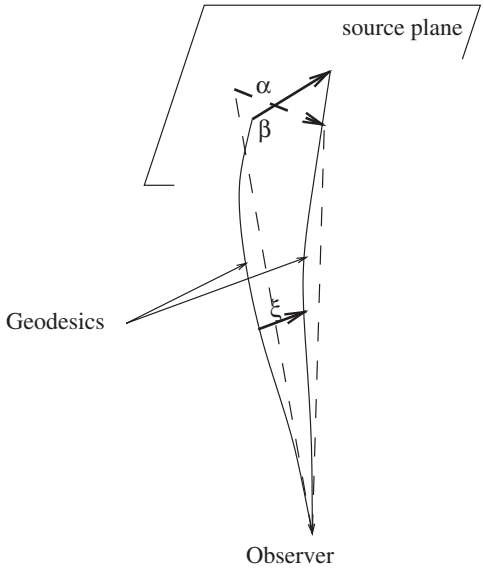

Figure 12. Sketch showing the geometrical quantities that appear in equation (58) .

The master equation that governs the evolution of the distance between the geodesics, whose derivation goes beyond what can be presented in this paper, is given in [88]:

$$\frac{\mathrm{d}^2[a\,\mathcal{D}_{ij}(\boldsymbol{\beta},z)]}{\mathrm{d}\eta^2} = a(z)\mathcal{R}_{ik}(\boldsymbol{\beta},z)\mathcal{D}_{kj}(\boldsymbol{\beta},z), \tag{61}$$

where the derivatives are taken with respect to η,

$$\mathrm{d}\eta = -\frac{\mathrm{d}a}{H(a)} = -a\,\mathrm{d}t, \qquad \eta(z=0)=0 \tag{62}$$

with the boundary conditions,

$$\left(\mathcal{D}_{ij}\right)_{z=0} = 0; \qquad \left(\frac{\mathrm{d}\mathcal{D}_{ij}}{\mathrm{d}\eta}\right)_{z=0} = \frac{c}{H_0}. \tag{63}$$

The matrix $\mathcal{R}_{ij}$ represents the tidal effects. It can be written in terms of the gravitational potential ϕ given by

$$\Delta\phi = 4\pi G\bar{\rho}a^2\delta_{\mathrm{matter}}. \tag{64}$$

The Laplacian is taken with respect to the comoving angular distances. We have

$$\mathcal{R}_{ij} = -\frac{4\pi G\bar{\rho}}{H_0^2a^2}\begin{pmatrix}1 & 0\\ 0 & 1\end{pmatrix} - \frac{2}{H_0^2a^2}\begin{pmatrix}\phi_{,11} & \phi_{,12}\\ \phi_{,21} & \phi_{,22}\end{pmatrix}. \tag{65}$$

Since $8\pi G\bar{\rho}a^3 = 3H_0^2\Omega_0$ (e.g. equation (16)) for a homogeneous universe we have

$$\mathcal{R}_{ij}^{(0)} = -\tfrac{3}{2}(1+z)^5\Omega_0\delta_{ij}^K \tag{66}$$

(here the superscript (0) means that this is the value of $\mathcal{R}$ without perturbations). In this case the matrix $\mathcal{D}_{ij}$ is proportional to δ_{ij}^K and we have

$$\frac{\mathrm{d}^2[a\,\mathcal{D}_0(z)]}{\mathrm{d}\eta^2} = -\frac{3}{2}(1+z)^4\Omega_0\mathcal{D}_0(z). \tag{67}$$

In fact, we recover the comoving angular distance, which is given by

$$\mathcal{D}_0(z) = \frac{c}{H_0\sqrt{1-\Omega_0-\lambda_0}} \sinh\left[\sqrt{1-\Omega_0-\lambda_0}\int_0^z \frac{\mathrm{d}z'}{E(z')}\right], \tag{68}$$

with

$$E(z) = \frac{H(z)}{H_0} = \sqrt{\lambda_0 + (1+z)^2(1-\Omega_0-\lambda_0) + (1+z)^3\Omega_0}. \tag{69}$$

This integral has a closed form only when the cosmological constant, Λ, is zero.

6.2. The linearized equation of geometric optics

We can remark that equation (61) is not linear since $\mathcal{D}$ is not simply proportional to $\mathcal{R}$. This expresses the fact that the deformation of the angular distance is made all along the light trajectory by multiple deflections. Solving equation (61) is in general very complicated. It can, however, be handled when it is linearized. Let us assume we can expand $\mathcal{D}_{ij}$ with respect to the local density contrast:

$$\mathcal{D}_{ij}(z) = \mathcal{D}_0 + \mathcal{D}^{(1)}_{ij} + \cdots. \tag{70}$$

It implies that, to first order,

$$\frac{\mathrm{d}^2[a\,\mathcal{D}^{(1)}_{ij}(\boldsymbol{\beta}, z)]}{\mathrm{d}\eta^2} - a(z)\mathcal{R}^{(0)}_{ik}(\boldsymbol{\beta}, z)\mathcal{D}^{(1)}_{kj}(\boldsymbol{\beta}, z) = -3\Omega_0(1+z)^4\mathcal{D}_0(z)\varphi_{,ij}(\boldsymbol{\beta}, z) \tag{71}$$

with

$$\left(\mathcal{D}^{(1)}_{ij}\right)_{z=0} = 0, \qquad \left(\frac{\mathrm{d}\mathcal{D}^{(1)}_{ij}}{\mathrm{d}\eta}\right)_{z=0} = 0, \tag{72}$$

where we have defined the field φ such that,

$$\Delta\varphi = \delta_{\mathrm{mass}}(\boldsymbol{\beta}, z) = \frac{\Delta\phi}{4\pi G\bar{\rho}a^2}. \tag{73}$$

After elementary mathematical transformations, this gives,

$$\begin{aligned}\mathcal{D}^{(1)}_{ij}(\boldsymbol{\beta}, z) = \quad & -3\Omega_0\int_0^z \frac{\mathrm{d}z'}{E(z)}\frac{1}{\sqrt{1-\Omega_0-\lambda_0}}\sinh\left[\sqrt{1-\Omega_0-\lambda_0}\int_z^{z'}\frac{\mathrm{d}z''}{E(z'')}\right] \\ & \times (1+z')\mathcal{D}_0(z')\varphi_{,ij}(z').\end{aligned} \tag{74}$$

It can be rewritten by introducing the physical distance χ along the line-of-sight. We eventually have

$$\mathcal{A}^{-1}(z) = \mathrm{Id} - \frac{3\Omega_0}{(c/H_0)^2}\int_0^{\chi(z)} \mathrm{d}\chi' \frac{\mathcal{D}_0(z', z)\mathcal{D}_0(z')}{\mathcal{D}_0(z)}(1+z')\varphi_{,ij}(z'), \tag{75}$$

where $\mathcal{D}_0(z)$ and $\mathcal{D}_0(z, z')$ are the angular comoving distances. This equation actually gives the expression of the amplification matrix for a non-trivial background. We find that the amplification matrix is given by the superposition of lens effects of the different mass layers. We can say that the lens term is given by the gravitational potential, ϕ, that is, by the potential, the source term of which is given by the density contrast.

Note, finally, that this equation is valid in two limiting cases—either for a single lens plane with an arbitrary strength or the superposition of any number of weak lenses. This equation naturally extends the previous result (5) obtained for a single lens in a Euclidean background. The higher orders of equation (61) give the intrinsic lens coupling effects (i.e. their non-linear parts) generally found to be negligible.

6.3. The weak lensing regime

In the weak lensing regime the deformation of the background objects can be described by the amplification matrix and the components of its inverse are, in general, written as

$$\mathcal{A}^{-1} = \begin{pmatrix} 1-\kappa-\gamma_1 & -\gamma_2 \\ -\gamma_2 & 1-\kappa+\gamma_1 \end{pmatrix}, \tag{76}$$

taking advantage of the fact that it is a symmetric matrix. The components of this matrix are expressed in terms of the convergence, κ (a scalar field), and the shear, γ (a pseudo-vector field), with

$$\kappa = \tfrac{1}{2}\nabla^2\psi; \qquad \gamma_1 = \tfrac{1}{2}(\psi_{,11} - \psi_{,22}); \qquad \gamma_2 = \psi_{,12} \tag{77}$$

with

$$\psi = 2\frac{D_{\rm LS}}{D_{\rm OS}D_{\rm OL}}\phi. \tag{78}$$

The convergence describes the linear change of size and the shear describes the deformation. The consequences of such a transform can be decomposed into two aspects:

- *The magnification effect.* Lenses induce a change of size of the objects. As the surface brightness is not changed by this effect, the change of surface induces a direct magnification effect, μ. This magnification is directly related to the determinant of $\mathcal{A}$ so that,

$$\mu = \det(\mathcal{A}) = \frac{1}{(1-\kappa)^2 - \gamma^2}. \tag{79}$$

- *The distortion effect.* Lenses also induce a change of shape of the background objects. The eigenvalues of the matrix $\mathcal{A}^{-1}$ determine the direction and amplitude of such a deformation.

This is the effect which is actually used to reconstruct the shear field. What one actually measures is the shape angular correlation function (see [74] for an exhaustive presentation). The reconstruction mass maps from distortion fields is not a trivial issue. In a pioneering paper, Kaiser and Squires [59] showed that this is indeed possible even beyond the weak lensing regime, the problem being easy to formulate in the weak lensing regime (in the single lens approximation),

$$\nabla\kappa = -\begin{pmatrix} \partial_1 & \partial_2 \\ -\partial_2 & \partial_1 \end{pmatrix} \cdot \begin{pmatrix} \gamma_1 \\ \gamma_2 \end{pmatrix} \tag{80}$$

when $\kappa \ll 1$ and $\gamma_i \ll 1$. By simple Fourier transforms it is then possible to recover κ from a distortion map. An extension of this relation has been given in [60] beyond the linear approximation that relates the reduced shear to κ. The practical implementation of such methods is however difficult because of the complex shape of the surveys one has to deal with. Indeed, bad columns, edge effects, bright stars are all sources of contamination in weak lensing surveys that have to be masked out. Because the shear–convergence relation is non-local, the reconstruction of the convergence is then made extremely arduous when masks of all shapes and sizes are scattered over the survey area. Under such circumstances the reconstruction of convergence maps with reliable statistical properties is even more problematic!

6.4. Cosmic shear

The idea of using lensing effects to map the large-scale structure of the universe dates back to the early 1990s [22, 75, 58] when it had been realized that typical mass fluctuations in the universe at megaparsec scale and over could be mapped through such weak lensing measurements.

To show that, one should uncover the relation between the convergence and local density contrasts. This can be derived from equations (19) and (5),

$$\kappa(\gamma) = \frac{3}{2}\Omega_0 \int \mathrm{d}z_s n(z_s) \int \mathrm{d}\chi \frac{\mathcal{D}(\chi_s, \chi)\mathcal{D}(\chi)}{\mathcal{D}(\chi_s)} \delta_{\mathrm{mass}}(\chi, \gamma)(1+z). \tag{81}$$

In this relation the redshift distribution of the sources is normalized such that,

$$\int \mathrm{d}z_s n(z_s) = 1, \tag{82}$$

and all the distances are expressed in units of c/H_0. The relation (81) is then totally dimensionless.

From this equation it is obvious that the amplitude of κ is directly proportional to the density fluctuation amplitude and that the two-point correlation function of the κ field is related to the shape of the density power spectrum. The relation (81) also shows that κ depends on the cosmological parameters. There is a significant dependence in the expression for the distances but the dominant contribution comes from the overall Ω_0 factor.

The amplitude of the fluctuations of κ depends on the angular scale at which the convergence map is filtered. We can introduce the filtered convergence κ_θ, with

$$\kappa_\theta(\gamma) = \int \mathrm{d}^2\gamma' \kappa(\gamma + \gamma') W_\theta(\gamma'), \tag{83}$$

where W is the window function. Expressed in terms of the Fourier modes it reads,

$$\kappa_\theta(\gamma) = \int \mathrm{d}\chi\, w(z) \int \frac{\mathrm{d}^2\boldsymbol{k}_\perp}{2\pi} \frac{\mathrm{d}k_r}{(2\pi)^{1/2}} \delta(\boldsymbol{k}) D_+(z) \exp[\mathrm{i}\boldsymbol{k}_r \chi(z) + \mathrm{i}\boldsymbol{k}_\perp \cdot \gamma \mathcal{D}(z0)] W\left[k_\perp \theta \mathcal{D}(z)\right], \tag{84}$$

where the wave vector $\boldsymbol{k}$ has been decomposed into two parts k_r and $\boldsymbol{k}_\perp$, which are respectively along the line-of-sight and perpendicular to it. The computation of the rms of κ_θ is analytic only in the small angle approximation and reads as follows:

$$\langle \kappa_\theta^2 \rangle = \int \mathrm{d}\chi\, w^2(\chi) \int \frac{\mathrm{d}^2\boldsymbol{k}}{2\pi} P(k) W^2(k_\perp \theta \mathcal{D}). \tag{85}$$

For realistic models of the power spectrum (e.g. [6]), it roughly gives [15],

$$\langle \kappa_\theta^2 \rangle^{1/2} \approx 0.01\, \sigma_8\, \Omega_0^{0.8}\, z_s^{0.75} \left(\frac{\theta}{1^\circ}\right)^{-(n+2)/2}. \tag{86}$$

One can note the strength of the dependence on the redshift of the sources. This was first stressed in [104] where it is pointed out that the Ω_0 dependence is roughly given by the Ω value at the redshift of the sources. These results are slightly affected by the introduction of non-linear effects in the shape of the power spectrum [75, 57]. Note also that the rms of κ_θ^2 is also the one of the shear field at the same scale so that the former can be directly obtained from the latter.

Are the effects from large-scale structures actually measurable? It can only be done in a statistical way. The idea is that towards some celestial direction the tiny deformations induced on background galaxies by the intervening mass fluctuations are roughly the same. Although they cannot be detected on a single object because of the galaxy intrinsic shape fluctuations, they can be detected from the statistical analysis if those intrinsic shape fluctuations are independent of each other. They then behave as a Poisson noise. Whether the gravitational effects can then be detected depends on the number density of background objects for which shape matrices are measurable. In current deep galaxy surveys the typical mean number density

of objects is about 30 arcmin^{-2}. The precision of the measured distortion at the degree scale is then about,

$$\Delta_{\rm noise}\kappa = \frac{0.3}{\sqrt{30 \times 60^2}} \approx 10^{-3}, \tag{87}$$

for an intrinsic ellipticity of sources of about 0.3. This number is to be compared with the expected amplitude of the signal coming from the large-scale structures, equation (86). It is clearly seen that, in domain cells of a few arc-minutes, detection of the cosmic shear signal is possible. The first reports of such detections came in early 2000 [101, 5, 105, 61].

6.5. Observations

To date the observational situation is as described in figure 13, which displays the amplitude of the cosmic shear filtered in cells of increasing radius as derived by different teams. There is no doubt that a signal of cosmic origin has been detected!

The cosmological constraints that can be derived from these observations are twofold and can be appreciated from equation (86). One can indeed see that the amplitude of the fluctuations depend both on σ_8 and Ω_0 in a fashion similar to that for galaxy clusters. The constraints obtained from weak lensing observations are actually in good agreement with the result of equation (55). Incidently the good match between these two results implies that the initial density fluctuations should not be too far from Gaussian so that the PS calculations are valid. These results confirm those obtained from galaxy catalogues concerning the amplitude of the density fluctuations. Together with the amplitude of the CMB temperature anisotropies, they point towards the existence of a cold dark matter component, whose amount is below the critical density value.

The weak lensing observations can, however, offer much more. In particular, it is possible to separate the amplitude of the power spectrum from the cosmological parameters. A simple

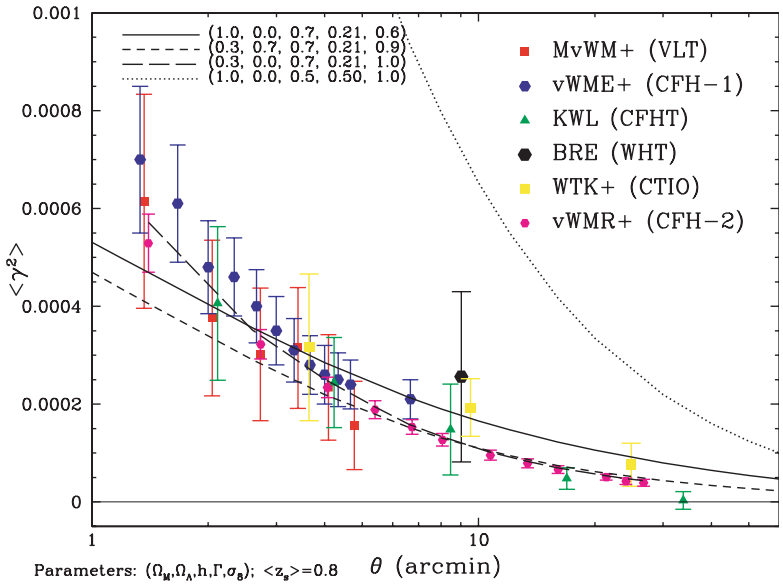

Figure 13. The amplitude of the cosmic shear at various angular scales.

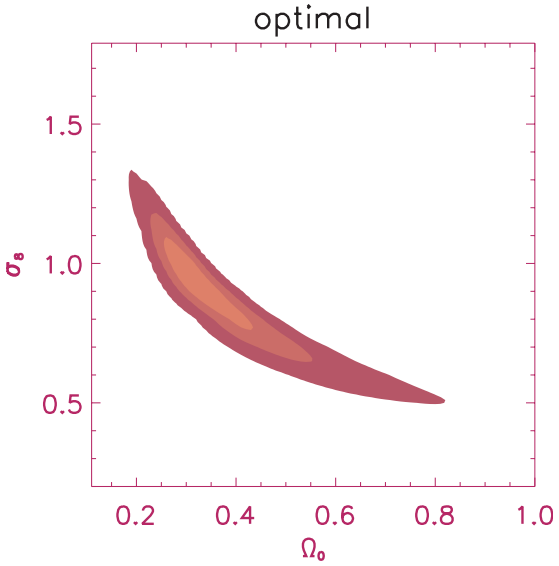

Figure 14. Joint constraint on Ω and σ_8 from weak lensing observations [102].

examination of equation (81) shows that this can only be the case if effects beyond the linear regime are considered. Indeed, it appears that for a given value of σ_κ, the density field should be strongly evolved in the non-linear regime when Ω_0 is low.

The consequences of this are twofold. The non-linearities change the angular scale at which the non-linear dynamics starts to amplify the growth of structures. This effect was investigated in more detail by Jain and Seljak [57] who showed that the emergence of the non-linear regime is apparent in the shape of the angular two-point function. This leads to joint determination of σ_8 and Ω [102] (see figure 14).

This effect is, however, quite subtle. It might be difficult to detect independently of peculiarities in the shape of the initial power spectrum. Another interesting aspect is that non-linear effects induce non-Gaussian features due to mode couplings. These effects have been studied extensively in perturbation theory and in phenomenological models, and valuable analytical results have been obtained. The detection of what appears to be a genuine non-Gaussian feature in a weak lensing survey has even been reported quite recently [14]. We will go back to these issues in the next section.

7. Challenging issues for a precision cosmology era

Comparisons between the observed power spectrum and theoretical predictions for CDM like spectra certainly show that the growth feature of the model that theorists have derived—gravitational instabilities mainly driven by a cold dark matter component—is correct. New generations of surveys are, however, going to allow much more detailed comparisons, subjecting the model to detailed scrutiny. Still open questions concern the exact nature of the initial conditions, namely, to which levels they are Gaussian, which is intimately related to tests of the gravitational instability scenario; the precise measurement of the vacuum energy density, its equation of state and eventually its redshift dependence.

The latter issue is far reaching since it questions our understanding of physics at a very fundamental level. In the following, we explain why the detection of an accelerating universe

is so challenging and what the observational means that we have at our disposal are, to tackle this issue.

7.1. What is the nature of dark energy?

From the viewpoint of observational cosmology the dark energy component that has been detected behaves strictly as a pure cosmological constant whose energy density represents today about 70% of the critical energy density. This fact relies on basically two concordant sets of observations. One is based on the measurement of the position of the Doppler peaks on the last scattering surface. As mentioned previously, at sub-horizon scales the plasma fluid starts to undergo acoustic oscillations that are now visible from the shape of the CMB anisotropy power spectra. It is then easy to understand that the position of the first peak is then the angular size of the sound speed horizon on the last scattering surface. This angle is given by

$$\theta_{\rm peak} = \frac{\eta_{\rm Sound-horizon}}{(1+z_*)d_A(z_*)}, \tag{88}$$

where $\eta_{\rm Sound-horizon}$ is given by the past time integral of the sound speed, v_s,

$$\eta_{\rm Sound-horizon} = \int^{\eta_*} {\rm d}\eta\, v_s = \int^{\eta_*} {\rm d}\eta\, \frac{1}{3(1+3\rho_b/(4\rho_\gamma))}, \tag{89}$$

where η is the conformal time and η_* is the value of η at the last scattering surface. It clearly shows that the angular size of the temperature patches on the last scattering surface depends on the cosmological parameters in a precise way. Its measurement essentially gives the angular distance to the last scattering surface, which can be summarized as one degeneracy line in an $\Omega_{\rm matter}$–Ω_Λ plane.

The observational constraints coming from Boomerang observations [78] are summarized in figure 15 as a blue (small shaded) area. They clearly indicate that the universe is close to flat ($\Omega_{\rm matter}+\Omega_\Lambda = 1$). This is to be contrasted to what has been gathered from the observations we have described in the previous sections, whether it is from the matter content of galaxy

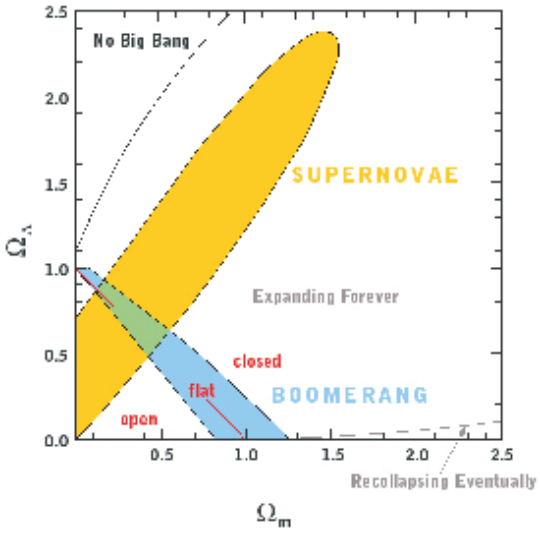

Figure 15. Current constraints on the $\Omega_{\rm matter}$–Ω_Λ values from CMB observations (blue (small shaded) area) and supernovae luminosity distances (orange (large shaded) area).

clusters or the parameter shape of the galaxy density power spectrum, all of which indicate that dark matter only accounts for about one-third of the critical density. The difference can only be explained if there exists an un-clustered form of cosmic fluid that carries the missing energy density.

The other piece of evidence that favours the existence of the dark energy is more direct. It comes from the observations of distant supernovae whose luminosities are assumed to be intrinsically known. The measurement of the apparent luminosities of distant supernovae then make it possible to detect the redshift evolution of the angular distance, the evolution of the latter depending on the matter/energy content of the universe. The current constraints are presented in figure 15 as an orange (large shaded) area. These two sets of observations can clearly be reconciled if and only if there exists a non-zero cosmological constant, or something that can play a similar role.

The existence of a non-zero vacuum energy density poses a range of different problems. First of all it has to be remarked that the time at which the energy density of this component is comparable to the matter energy density can happen only at a peculiar moment in cosmological history. It is then somehow coincidental that we observe the universe at precisely this time. No convincing explanation for this coincidence has been given.

The existence of a non-zero cosmological constant is also problematic from a high-energy physics point of view. Interpreting the cosmological constant as a vacuum energy density, calls for interpreting it as the zero point value of the quantum fields with which the universe is filled. The estimated vacuum energy from this point of view is, however, far off from what is measured, by more than hundred orders of magnitude. Even if we could explain this strictly zero value for the cosmological constant citing symmetry reasons yet to be uncovered, this large discrepancy in terms of orders of magnitude is very uncomfortable. Theorists are also uncomfortable with a late time de Sitter space that can hardly be accommodated with a superstring theory background.

One way out is to assume that what is observed may not be due to the true quantum vacuum but due to a transitional cosmological state. This is basically the idea of the quintessence models where the required equation of state is obtained in a manner similar to the inflation models. In this case the dark energy identifies with the energy density of a scalar field rolling down a potential, the difference being that the mass of this field has to be extremely small. The motion equation for the field value is the following,

$$\ddot{Q} + 3H\dot{Q} = -\frac{\partial V}{\partial Q}, \tag{90}$$

and models of quintessence are characterized by a choice of potentials. The simplest model is for an inverse power law model,

$$V(Q) = M^{4+\alpha} Q^{-\alpha}, \tag{91}$$

where M is the energy scale of the field and α is positive. This is also the simplest model exhibiting a tracking solution. In particular, it is very hard, with this potential, to get an equation of state $\omega_Q < -0.7$ while keeping a reasonable (from the high-energy physics point of view) energy normalization for M if $\Omega_\Lambda = 0.7$ today. Note that for such a potential the vacuum equation of state of the attractor solution is given by

$$\omega_Q = \frac{-2 + \alpha\omega_B}{\alpha + 2}, \tag{92}$$

where ω_B is the equation of state parameter of the background fluid ($\frac{1}{3}$ for a radiation dominated universe, 0 for a matter dominated universe). In the following we will consider the case $\alpha = 2$, which gives $\omega_Q \sim -0.6$ today, marginally consistent with the supernovae observations, although it leads to an unrealistically low energy scale for M.

Among the possible extensions of this model one particularly interesting form, from a phenomenological point of view, is the SUGRA model, proposed by Brax and Martin [26, 27], whose potential is

$$V_{\rm Sugra}(Q) = \frac{M^{4+\alpha}}{Q^{\alpha}} \exp\left[4\pi \frac{Q^2}{M^2_{\rm Planck}}\right]. \tag{93}$$

The corrective factor is motivated by the fact that, in the Ratra–Peebles scenario, the field naturally reaches the Planck scale at low redshift. If the quintessence potential is to be derived from models beyond the standard model of particle physics, which are expected to include supergravity properties, it is natural to expect supergravity corrections in the shape of the potential which appears as the exponential factor. This model appears to be of particular interest since its predictions are in good agreement, for a wide range of parameters, with the SNIa measurements. This potential with, for instance, either $\alpha = 6$ or 11 leads to an equation of state $\omega_Q \sim -0.8$ at zero redshift. With these choices of parameters the energy scale M ranges from 10^6 to 10^{11} GeV, which does not contradict our knowledge of high-energy physics (see figure 16).

The two quintessence models, equations (91) and (93), have the same tracking solution and the equation of state parameter is thus the same (given by equation (92)), on it. Differences between the two models arise when the field leaves the tracking solution. At this time, the field value is of the order of the Planck mass, and the SUGRA correction of the latter models starts to dominate. This SUGRA correction cures the problems encountered by the Ratra–Peebles potential by quickly slowing down the field as it rolls down thus providing a smaller equation of state parameter [27, 26].

Interestingly, the mere existence of the tracking solution implies that the quintessence fluctuations must have been damped during the cosmic evolution. Therefore, the impact of quintessence models of the shapes of the CMB anisotropy power spectrum or that linear density contrast can only be weak. It has been examined in detail for different models of high-energy physics tracking potentials [36, 28]. It has been found that at the redshift of recombination the dark energy fluid is sub-dominant and has only significant super-horizon fluctuations. Quintessence effects are therefore reflected only in a modest change of the Sachs–Wolfe plateau, an effect difficult to be unambiguously detected because of the importance of the cosmic variance.

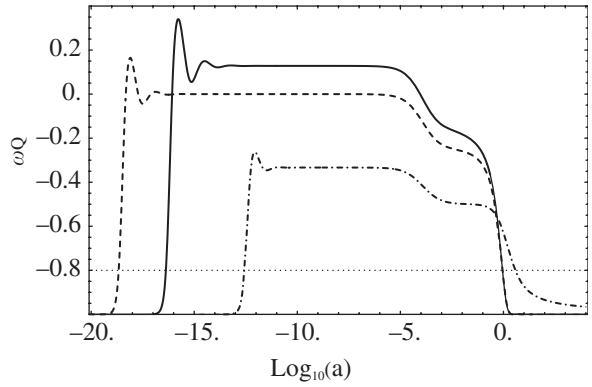

Figure 16. The evolution of the vacuum equation of state as a function of the expansion parameter a for different cosmological models. The dotted line corresponds to a vacuum equation of state, $p = -0.8\rho$ and the dot-dashed line to a Ratra–Peebles solution with $\alpha = 2$ (equation (91)); the dashed line corresponds to a SUGRA behaviour (equation (93)) to $\alpha = 6$ and the solid line with $\alpha = 11$. The amplitude of the quintessence potentials is such that $\Omega_{\rm matter} = 0.3$ at $z = 0$ in all cases.

Evidences for a cosmological constant may, however, be due to other mechanisms. The observations may mean, for instance, that the very law of gravity is no more valid at the Hubble scale. It has indeed never been explicitly tested at these scales. That might happen in particular in exotic models of cosmology inspired by superstring theories where there exist extremely large space dimensions that cannot be experienced but through gravity.

The understanding of the nature of the observed 'dark energy' thus involves far-reaching issues. One way to shed light on them would be to measure accurately the equation of state of the dark energy component. If it were to depart from the one of a pure cosmological constant, it would be a major discovery for fundamental physics.

Observational tools to explore this physics are at least twofold. One is the measurements of distances using of distant supernovae. In figure 17 we show how a collection of a few thousands of supernovae could help in distinguishing different models. In this plot the Sugra model corresponds to the thin solid line. Other lines correspond to other models that have been advocated in the literature (but it is beyond the scope of this general paper to review all of them): the thin short dashed line is the trapped minimum model, the thin dot–short dashed line is from the brane inspired potential, the thin short-dashed–long-dashed line from the potential which involves two exponentials, the thick short dashed line from the periodic potential, the thick long dashed line from the pure exponential, the thick solid line from the Pseudo Nambu–Gotu Boson potential, the thin long dashed line from the exponential tracker solution (underneath $w = -1$), and the thick dotted line from the inverse tracker.

Other probes of the energy content of the universe and of its geometrical properties are the large-scale structure measurements. CMB observations, although very important in the

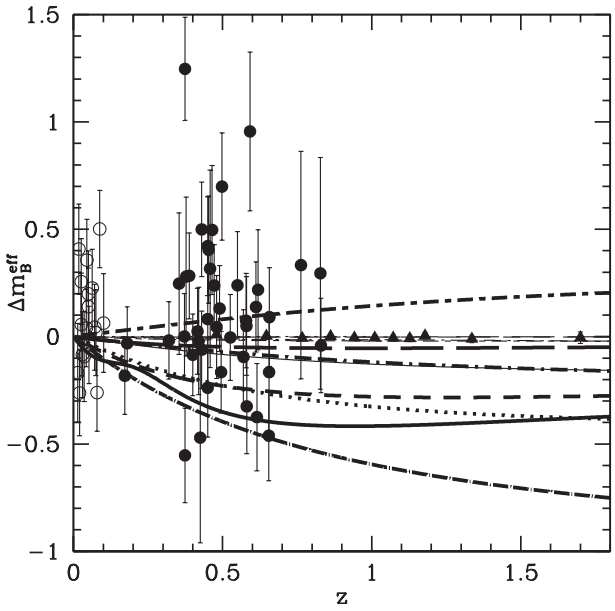

Figure 17. The relative magnitude with respect to a cosmology with $\Omega_m = 0.3$ and $\Omega_\Lambda = 0.7$. The solid triangles are the binned data points with errorbars from the SNAP type specifications [110]. Open circles are for the Calán/Tololo data [49] and the solid triangles for the SCP SCP data points [83]. The curves correspond to a set of various theoretical models (see text). The thick dot–short dashed line is a cosmological constant model with $\Omega_\Lambda = 0.6$ and the thick short-dashed—long-dashed line a model with $\Omega_\Lambda = 0.8$. The thick long dashed line is the 'Standard Cold Dark Matter' model with $\Omega_m = 1.0$, which is clearly ruled out by the current data.

exploration of the physics of the early universe, can provide only very little for testing the physics of the universe at low redshift. Basically, its interest reduces to a single value constraint that almost identifies with the angular distance to the last scattering surface. To get a more detailed insight into the low redshift physics of the universe, local surveys will have to be scrutinized in their finest details and an excursion into the physics of gravitational clustering is required for this. This is the aim of the next sections.

7.2. Tests of the large-scale gravity law

Let us first explore what could be the low redshift phenomenological consequences of a change of gravity laws. Lensing surveys because they are direct maps of gravitational potentials, offer a precious window for this kind of effects. To guide our exploration, such un-standard gravity law models should be put in the context of recent low energy phenomenological developments that have been inspired by the introduction of branes in superstring theories [4, 86, 20]. Branes lead to concepts of higher dimensional space-times in which the interaction gauge fields are localized on a 3-brane (i.e. a 3 + 1 dimension spacetime) whereas gravity propagates in all dimensions. In any of such string inspired models, one expects both the existence of Kaluza–Klein gravitons, implying a non-standard gravity on small scales, and light bosons, which can manifest as a new fundamental small-scale force. But the existence of extra dimensions might also be revealed by non-standard gravity laws that depart large-scales. For instance, if there are neighbouring branes, the inter-brane distance then appears as a new scale (exponentially large compared to the small distance scale) above which gravity is non-standard [46, 64]. This will be the case whenever gravity is not perfectly localized on the brane, that is, when photons can leak out of it [32]. This has been proposed as a possible explanation of the observed acceleration of the universe. This certainly is quite a speculative idea, but may not be so compared to many others!

So let us assume that Newton's law is violated above a given scale r_s and explore its phenomenological consequences for the growth of structures. Equation (20), that is, the expression of the force exerted between two masses at a distance r is changed. It now derives from $\Phi = \Phi_N f(r/r_s)$ where $f(x) \to 1$ when $x \ll 1$. This encompasses, for instance, the potential considered in [46, 21] for which $f(x) = 1/(1+x)$ (in that case $f \propto 1/x$ and five-dimensional gravity is recovered at large distance). This phenomenological description leads to

$$\phi(\boldsymbol{x}) = -G\rho a^2 \int \mathrm{d}^3\boldsymbol{x}' \frac{\delta(\boldsymbol{x}')}{|\boldsymbol{x}-\boldsymbol{x}'|} f\left(\frac{|\boldsymbol{x}-\boldsymbol{x}'|}{x_s}\right), \tag{94}$$

with $\boldsymbol{r} = a\boldsymbol{x}$ and which, making use of $\Delta[f(x)/x] = -4\pi\delta^{(3)}(\boldsymbol{x}) + f_s(x/x_s)$ with $f_s(x/x_s) \equiv (\partial_x^2 f)/x$ gives

$$\Delta\Phi = \Delta\Phi_N - G\rho a^2 \int \mathrm{d}^3\boldsymbol{x}' \delta(\boldsymbol{x}'+\boldsymbol{x}) f_s\left(\frac{x'}{x_s}\right). \tag{95}$$

In Fourier space, equation (95) reads

$$-k^2\widehat{\Phi}(k) = 4\pi G\rho a^2 \widehat{\delta}(k) f_c(kr_s) \tag{96}$$

from which we deduce that

$$\mathcal{P}_{\Delta\Phi}(k) = \left(4\pi G\rho a^2\right)^2 \mathcal{P}_\delta(k) f_c(kr_s)^2, \tag{97}$$

where $f_c(kr_s) \equiv 1 - 2\pi^2 f_s(kr_s)$, $f_s(kr_s)$ being the Fourier transform of $f_s(r/r_s)$. A method of testing the validity of Newton's law is thus to test the validity of equation (19), which is possible if one can measure δ and Φ independently.

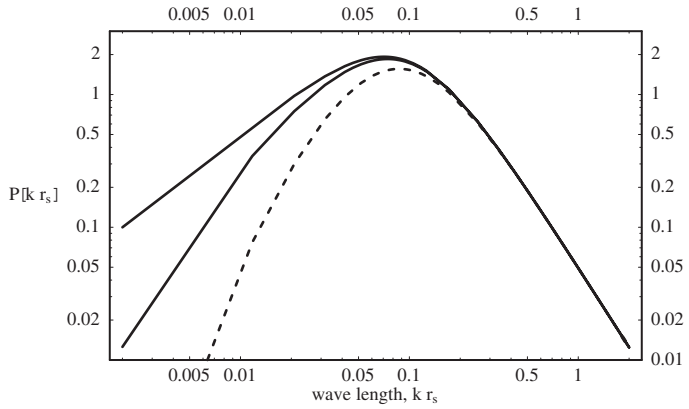

Figure 18. Example of discrepancy between cosmic shear power spectrum (- - - -) and galaxy count power spectrum (——) in the case of departure from four-dimensional gravity at large scales [100].

To illustrate this discrepancy we consider the growth of the perturbations on scales from ten to some hundreds of Mpc in a modified gravity scenario. For that purpose, we assume that the standard behaviour of the scale factor is recovered (i.e. it behaves according to the standard Friedmann equations). The equation of evolution of the density contrast, δ_k, taking advantage of the fact that the relation between δ and Φ is local in Fourier space (see equation (96)), is then

$$\ddot{\delta}_k - 2H\dot{\delta}_k - \frac{3}{2}H^2\Omega(t)\,f_c\left(k\frac{r_s}{a(t)}\right)\delta_k = 0. \tag{98}$$

Looking for a growing mode as $\delta_k \propto t^{\nu_+(k)}$ in a Einstein–de Sitter matter dominated universe ($\Omega = 1,\ H = 2/3t$) gives a growing solution such that $\nu_+(k) \to \frac{2}{3}$ for $kx_s \gg 1$ and $\nu_+(k) \to 0$ for $kx_s \ll 1$. At large scales the fluctuations stop growing mainly because gravity becomes weaker and weaker. The resulting power spectra are depicted in figure 18 assuming that $f(x) = 1/(1+x)$ and for $r_s = 50\,\mathrm{h}^{-1}$ Mpc. It can be observed that the power spectrum of the potential fluctuations, as can be observed from weak lensing surveys, and the one for the density field differ at large scales. This discrepancy is a direct signature of a modified law of gravity, although this deviation is somewhat model dependent (it depends in particular on the cosmological parameters). It is also to be noted that we are here in a regime where the biasing mechanisms (i.e. the fact that galaxies do not necessarily trace faithfully the matter field, see paragraph 5.2) should not hamper the completion of this test, the bias factor indeed being found to have an insignificant scale dependence at such scales [77].

Unconventional gravity laws might be betrayed by such observations, not the introduction of a cosmic component with some exotic equation of state.

7.3. Perturbation theories for a detailed insight into gravitational instability dynamics

The driving idea for perturbation theory investigations is that it is now possible to map the large-scale mass fluctuations in the universe in exquisite detail. In the previous sections we have seen that we have a good understanding of the linear regime for the growth of structure. This is not so much the case as soon as the non-linear couplings start to play a role. This would though be of crucial importance to gain insights into the dynamics in this regime because a fair fraction of the data actually concerns this regime carrying precious information on the initial

conditions, the background evolution, etc. Partial insights into this regime have been obtained from the use of perturbation theory [17], the basis of which we present in the following sections.

7.3.1. The basis of the perturbation theory calculations. Technically the perturbation theory hypothesis amounts to assuming that the local density contrast can be expanded with respect to the initial density fluctuations [82, 37, 45, 11]

$$\delta_{\rm matter}(\boldsymbol{x}) = \delta^{(1)}_{\rm matter}(\boldsymbol{x}) + \delta^{(2)}_{\rm matter}(\boldsymbol{x}) + \cdots, \tag{99}$$

where $\delta^{(1)}_{\rm matter}(\boldsymbol{x})$ is proportional to the initial density field (this is the term the behaviour of which we considered in the first sections), $\delta^{(2)}_{\rm matter}(\boldsymbol{x})$ is quadratic, etc.

The expression for the higher order terms can be derived from the equations of motion. Let us first consider an Einstein–de Sitter universe, for which $\Omega_m = 1$ and $\Omega_\Lambda = 0$. In this case the Friedmann equation, equation (15), implies $a \propto t^{2/3}$, $H(t) = 2/(3t)$, and scaling out an overall factor of H from the velocity field brings equations (24) and (25) into a homogeneous form in $a(t)$. As a consequence, these equations can formally be solved with the following joint perturbative expansion [45, 56, 71] for the density field and the velocity divergence field $\theta \equiv -\nabla \boldsymbol{u}/(aH)$, whether it is in real space or in Fourier space,

$$\delta(\boldsymbol{k}, t) = \sum_{n=1}^{\infty} a^n \delta_n(\boldsymbol{k}), \qquad \theta(\boldsymbol{k}, t) = \sum_{n=1}^{\infty} a^n \theta_n(\boldsymbol{k}). \tag{100}$$

In the previous equation only the fastest growing mode is taken into account. Remarkably, it implies that the PT expansions defined in equations (99) and (100) are actually expansions with respect to the linear density field with time independent coefficients. At small a the series are dominated by their first term, and since $\theta_1(\boldsymbol{k}) = \delta_1(\boldsymbol{k})$ from the continuity equation, $\delta_1(\boldsymbol{k})$ completely characterizes the linear fluctuations.

The equations of motion, equations (24) and (25), determine $\delta_n(\boldsymbol{k})$ and $\theta_n(\boldsymbol{k})$ in terms of the linear fluctuations to be

$$\delta_n(\boldsymbol{k}) = \int \mathrm{d}^3\boldsymbol{q}_1 \ldots \int \mathrm{d}^3\boldsymbol{q}_n \delta_D(\boldsymbol{k} - \boldsymbol{q}_{1\ldots n}) F_n(\boldsymbol{q}_1, \ldots, \boldsymbol{q}_n) \delta_1(\boldsymbol{q}_1) \ldots \delta_1(\boldsymbol{q}_n), \tag{101}$$

$$\theta_n(\boldsymbol{k}) = \int \mathrm{d}^3\boldsymbol{q}_1 \ldots \int \mathrm{d}^3\boldsymbol{q}_n \delta_D(\boldsymbol{k} - \boldsymbol{q}_{1\ldots n}) G_n(\boldsymbol{q}_1, \ldots, \boldsymbol{q}_n) \delta_1(\boldsymbol{q}_1) \ldots \delta_1(\boldsymbol{q}_n), \tag{102}$$

where F_n and G_n are homogeneous functions of the wave vectors $\{\boldsymbol{q}_1, \ldots, \boldsymbol{q}_n\}$ with degree zero. They are constructed from the fundamental mode coupling functions $\alpha(\boldsymbol{k}_1, \boldsymbol{k}_2)$ and $\beta(\boldsymbol{k}_1, \boldsymbol{k}_2)$ that appear in the equations of motion when written in Fourier space:

$$\alpha(\boldsymbol{k}_1, \boldsymbol{k}_2) \equiv \frac{\boldsymbol{k}_{12} \cdot \boldsymbol{k}_1}{k_1^2}, \qquad \beta(\boldsymbol{k}_1, \boldsymbol{k}_2) \equiv \frac{k_{12}^2 (\boldsymbol{k}_1 \cdot \boldsymbol{k}_2)}{2 k_1^2 k_2^2}, \tag{103}$$

according to the recursion relations ($n \geqslant 2$, see [45, 56] for a derivation):

$$\begin{aligned} F_n(\boldsymbol{q}_1, \ldots, \boldsymbol{q}_n) = \sum_{m=1}^{n-1} \frac{G_m(\boldsymbol{q}_1, \ldots, \boldsymbol{q}_m)}{(2n+3)(n-1)} [&(2n+1)\alpha(\boldsymbol{k}_1, \boldsymbol{k}_2) F_{n-m}(\boldsymbol{q}_{m+1}, \ldots, \boldsymbol{q}_n) \\ &+ 2\beta(\boldsymbol{k}_1, \boldsymbol{k}_2) G_{n-m}(\boldsymbol{q}_{m+1}, \ldots, \boldsymbol{q}_n)], \end{aligned} \tag{104}$$

$$\begin{aligned} G_n(\boldsymbol{q}_1, \ldots, \boldsymbol{q}_n) = \sum_{m=1}^{n-1} \frac{G_m(\boldsymbol{q}_1, \ldots, \boldsymbol{q}_m)}{(2n+3)(n-1)} [&3\alpha(\boldsymbol{k}_1, \boldsymbol{k}_2) F_{n-m}(\boldsymbol{q}_{m+1}, \ldots, \boldsymbol{q}_n) \\ &+ 2n\beta(\boldsymbol{k}_1, \boldsymbol{k}_2) G_{n-m}(\boldsymbol{q}_{m+1}, \ldots, \boldsymbol{q}_n)], \end{aligned} \tag{105}$$

where $\boldsymbol{k}_1 \equiv \boldsymbol{q}_1 + \cdots + \boldsymbol{q}_m$, $\boldsymbol{k}_2 \equiv \boldsymbol{q}_{m+1} + \cdots + \boldsymbol{q}_n$, $\boldsymbol{k} \equiv \boldsymbol{k}_1 + \boldsymbol{k}_2$, and $F_1 = G_1 \equiv 1$.

For $n = 2$ we thus have

$$F_2(\boldsymbol{q}_1, \boldsymbol{q}_2) = \frac{5}{7} + \frac{1}{2}\frac{\boldsymbol{q}_1 \cdot \boldsymbol{q}_2}{q_1 q_2}\left(\frac{q_1}{q_2} + \frac{q_2}{q_1}\right) + \frac{2}{7}\frac{(\boldsymbol{q}_1 \cdot \boldsymbol{q}_2)^2}{q_1^2 q_2^2}, \tag{106}$$

$$G_2(\boldsymbol{q}_1, \boldsymbol{q}_2) = \frac{3}{7} + \frac{1}{2}\frac{\boldsymbol{q}_1 \cdot \boldsymbol{q}_2}{q_1 q_2}\left(\frac{q_1}{q_2} + \frac{q_2}{q_1}\right) + \frac{4}{7}\frac{(\boldsymbol{q}_1 \cdot \boldsymbol{q}_2)^2}{q_1^2 q_2^2}. \tag{107}$$

Explicit expressions for the kernels F_n and G_n can be obtained to any arbitrary order. For instance, F_3 and F_4 are given in [45].

The physical interpretation is the following. The functions F_n, which can be directly measured as we will see in the next paragraph, bear some information about the gravitational instability mechanism. In particular, they have a specific geometric dependence that can be explicitly detected. It is also to be noted that they are, to a very good accuracy, independent of the cosmological parameters, or more generally, independent of the matter and energy content of the universe [17, 25, 24, 12, 7, 44].

7.3.2. Phenomenological consequences. Consequences of these terms are multifold. They change the shape of the power spectrum and this aspect is still difficult to grasp because it rapidly becomes a completely non-linear problem. The next to leading order terms also induce non-Gaussian features in the cosmic density field, which can be observed, for instance when, high order correlation functions are measured.

Thus, at leading order in a perturbative approach, the three-point correlation function takes a non-trivial shape that can be written in terms of the F_2 function. It is easier to write it down in Fourier space where third order ensemble averages define the bispectrum, $B(\boldsymbol{k}_1, \boldsymbol{k}_2, \tau)$,

$$\langle \delta(\boldsymbol{k}_1)\delta(\boldsymbol{k}_2)\delta(\boldsymbol{k}_3)\rangle_c = \delta_D(\boldsymbol{k}_1 + \boldsymbol{k}_2 + \boldsymbol{k}_3)\; B(\boldsymbol{k}_1, \boldsymbol{k}_2). \tag{108}$$

Anticipating the results of perturbation theory, it is convenient to define the reduced bispectrum Q as [40, 37]

$$\tilde{Q} \equiv \frac{B(\boldsymbol{k}_1, \boldsymbol{k}_2, \tau)}{P(k_1, \tau)P(k_2, \tau) + P(k_2, \tau)P(k_3, \tau) + P(k_3, \tau)P(k_1, \tau)}. \tag{109}$$

It has the desirable property that it is scale and time independent to lowest order (tree-level) in non-linear PT,

$$\tilde{Q}^{(0)} = \frac{2F_2(\boldsymbol{k}_1, \boldsymbol{k}_2)P(k_1, \tau)P(k_2, \tau) + \text{cyc.}}{P(k_1, \tau)P(k_2, \tau) + P(k_2, \tau)P(k_3, \tau) + P(k_3, \tau)P(k_1, \tau)}, \tag{110}$$

where $F_2(\boldsymbol{k}_1, \boldsymbol{k}_2)$ denotes the second-order kernel obtained from the equations of motion. Recall that this kernel is very insensitive to cosmological parameters, as a consequence of this, the tree-level reduced bispectrum $\tilde{Q}^{(0)}$ is almost independent of cosmology [38, 52]. In addition, from equation (110) it follows that $\tilde{Q}^{(0)}$ is independent of time and normalization [37]. Furthermore, for scale-free initial conditions, $P_L(k) \propto k^n$, $\tilde{Q}^{(0)}$ is also independent of overall scale. For the particular case of equilateral configurations ($k_1 = k_2 = k_3$ and $\hat{k}_i \cdot \hat{k}_j = -0.5$ for all pairs), $\tilde{Q}^{(0)}$ is independent of spectral index as well, $\tilde{Q}^{(0)}_{\text{EQ}} = \frac{4}{7}$. In general, for scale-free initial power spectra, $\tilde{Q}^{(0)}$ depends on configuration shape through, e.g. the ratio k_1/k_2 and the angle θ defined by $\hat{k}_1 \cdot \hat{k}_2 = \cos\theta$. In fact, since bias between the galaxies and the underlying density field is known to change this shape dependence [39], measurements of the reduced bispectrum Q in galaxy surveys could provide a measure of bias that is insensitive to other cosmological parameters [38], unlike the usual determination from peculiar velocities, which has a degeneracy with the density parameter Ω_m (see figure 19).

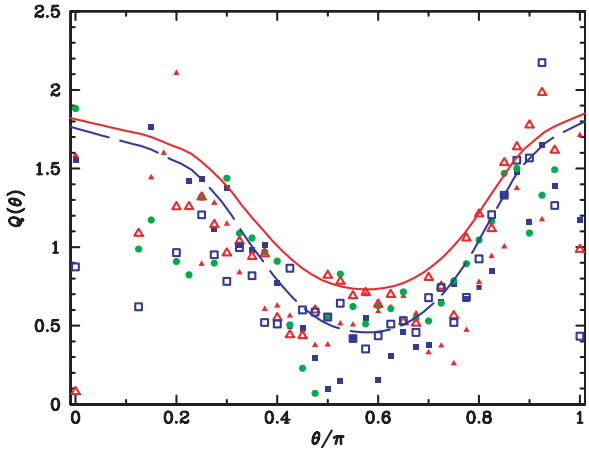

Figure 19. Dependence of the coefficient Q describing the three-point correlation function as measured in the PSCz survey. The overall shape is in agreement with what is expected from a perturbation theory approach.

7.4. Consequences for weak lensing surveys

Although galaxy surveys offer a precious way of probing the very law of gravity through the large-scale structure properties, precise analyses of such surveys ultimately suffer from the bias problem. Weak lensing surveys, on the other hand directly probe the mass distribution in the universe thus providing a better playground for detailed tests of the gravitational dynamics. Perturbation theory calculations presented in the earlier part can equivalently be undertaken for the local convergence field. Once again the perturbative expansion is made in terms of the initial density field,

$$\kappa(\gamma) = \kappa^{(1)}(\gamma) + \kappa^{(2)}(\gamma) + \cdots \tag{111}$$

The non-zero $\kappa^{(2)}$ term induces non-Gaussian effects that can be revealed, for instance, by the computation of the skewness, third moment, of κ_θ,

$$\langle \kappa_\theta^3 \rangle = \left\langle \left(\kappa_\theta^{(1)}\right)^3 \right\rangle + 3\left\langle \left(\kappa_\theta^{(1)}\right)^2 \kappa_\theta^{(2)} \right\rangle + \cdots \tag{112}$$

The actual dominant term of this expansion is $3\langle (\kappa^{(1)})^2 \kappa^{(2)} \rangle$ since the first term vanishes for Gaussian initial conditions. For the computation of such term one should plug in equation (81) the expression of $\delta^{(2)}_{\rm matter}$ derived from equation (106) and do the computations in the small angle approximation (and using specific properties of the angular top-hat window function [13]).

Eventually, perturbation theory gives the following result for a realistic power spectrum [15]:

$$s_3(\theta) \equiv \frac{\langle \kappa_\theta^3 \rangle}{\langle \kappa_\theta^2 \rangle^2} = 40\ \Omega_0^{-0.8}\ z_s^{-1.35}. \tag{113}$$

The origin of this skewness is relatively simple to understand: as the density field enters the non-linear regime the large mass concentrations tend to acquire a large density contrast in a small volume. This induces rare occurrences of large negative convergences. The under-dense regions tend, on the other hand, to occupy a large fraction of the volume, but can induce only moderate positive convergences. When the mean source of the redshift grows the skewness diminishes since the addition of independent layers of large-scale structures tends to dilute the non-Gaussian nature.

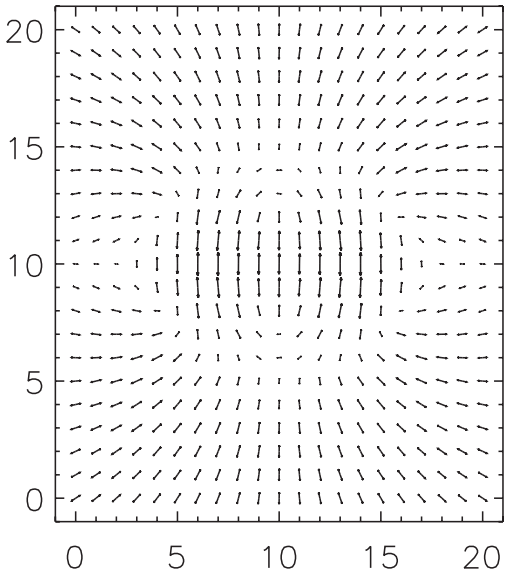

Figure 20. Shape of the shear three-point correlation function, equation (114) as a function of the $\boldsymbol{x}_3$ position for fixed $\boldsymbol{x}_1$ and $\boldsymbol{x}_2$ positions. The latter points are respectively at positions $(-4, 0)$ and $(4, 0)$ in the figure coordinates.

These results have been extended in the intermediate regime [103], in the non-linear regime [54]. Investigations are now being conducted that aim to explore quantities that are directly accessible in shear maps such as some combinations of shear three-point correlation functions [16, 107, 90, 97]. They could serve as means for detecting non-Gaussian features in shear surveys without having to rely on mass reconstruction.

The crucial issue in this exploration is that the shear three-point correlation function vanishes at zero separation for obvious symmetry reasons. One then has to consider a point configuration at finite distances. Different strategies have been put forward. The one that was finally tested against actual data is given by

$$\hat{\xi}_3 = \left\langle \left(\gamma_{\boldsymbol{x}_1} \cdot \gamma_{\boldsymbol{x}_2}\right)\gamma_{\boldsymbol{x}_3} \right\rangle \tag{114}$$

which exhibits non-trivial patterns (see figure 20) obtained here for an open-CDM model [16].

From the coherent pattern that can be noticed at the centre of this figure, it had been possible to design a detection strategy that led to the first detection of non-Gaussian features in a cosmic shear data survey [14]. The amplitude and shape of the observed signal are in good agreement with what is expected in a Λ-CDM model. Although these recent results are certainly too premature to allow scientific exploitation, it is now clear that weak lensing surveys will soon be large enough to provide a way to break the degeneracy between the amplitude of the density fluctuations, σ_8, and the matter density parameter of the universe, Ω_{matter}. In the context of dark energy searches this is a valuable tool. It means that constraints on the matter density parameter of the universe can be obtained on the sole basis of the amount of non-Gaussian features induced through the density fluctuation growth and thus in a way that depends only marginally on the vacuum equation of state. It is, however, possible to have a more direct access to the vacuum equation of state.

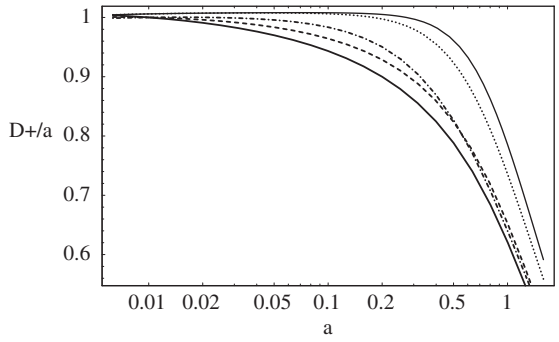

Figure 21. Linear growth rate of the cosmological density perturbations for different models of the cosmological vacuum equation of state standard model (——), Sugra model (——), Ratra–Peebles models (· · · · · ·), from [7] .

7.5. Weak lensing to probe the nature of dark energy

Better insights into the vacuum equation of state can be obtained from the growth rate of the fluctuations as a function of redshift. The shape of the resulting power spectrum of the convergence field is, in particular, sensitive to the whole matter content of the universe and its equation of state. The reason is simple. The linear growth rate of the fluctuations depends jointly on the time evolution of the expansion factor and on the matter density as it appears in equation (26). The time at which the density fluctuations enter the non-linear regime at various scales is therefore dependent on the cosmological parameters as a whole.

This appears clearly in figure 21, where the linear growth rate D_+ in units of a is compared to unity (which would correspond to an Einstein–de Sitter universe) in different models that contain the same amount of dark energy. The growth clearly starts to slow down at much earlier times in the case of the quintessence models, either in the Ratra–Peebles model (thick dotted lines), where the vacuum energy is that of the scalar field rolling down an inverse power law potential, or even more strikingly in 'Sugra' models, which incorporate supergravity corrections that modify the shape of the potential [27, 26] (thick dotted line), equation (93). Such a behaviour is due to the fact that in quintessence models the fraction of energy in the dark energy can be significant over a long period. The consequences can be seen in figure 22 which shows the projected matter power spectra for these different models of cosmological vacuum. The resulting power spectra are compared to what one would have obtained in the case of the cosmological vacuum being described by a pure cosmological constant. The Ratra–Peebles or Sugra models clearly depart from the standard scenario and in a way that is quite different from a change of Ω_0. Such a variation should be within the detection range of the next generation of weak lensing surveys such as the CFHTLS [109], points with error bars.

These results illustrate the fact that weak lensing observations can be used to infer fruitful information on the matter content of the universe. It is to be noted, however, that the scales which are better at discriminating the different models correspond to the intermediate regime where our theoretical understanding of the physics is less secure. It calls for great effort in the coming years towards a better understanding of that regime, whether it is from rigorous perturbation theory calculations or from phenomenological models such as the halo models [29].

8. Conclusions

The existence of dark matter is now firmly established as it is supported by many concordant observations. Since the early indication from Zwicky's study, direct indications coming from

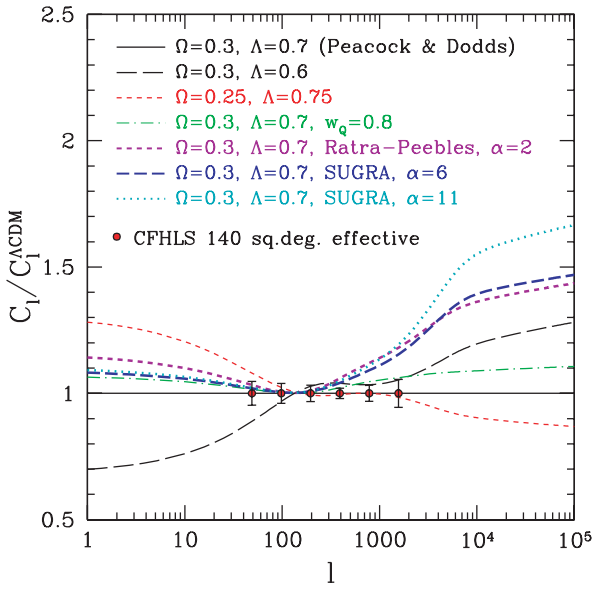

Figure 22. Convergence power spectrum for different hypotheses on the vacuum equation of state compared to a standard model, from [7]. The points with error-bars are the anticipated results and errors for a $140^{\circ 2}$ survey such as the CFHTLS survey [109] under development.

the observation of galaxy velocity profiles, or the observation of galaxy clusters, whether it is from their internal velocity dispersion or from their x-ray luminosity, have been confirmed over the last decades. The other convincing piece of evidence comes from the observations of the cosmological properties of the universe and its structure. The shape of the density fluctuation power spectrum betrays both the existence of dark matter and that it cannot account for an energy density that equals the critical density. All the best understood cosmological observations now form a concordance model in which 30% of the critical energy density is from matter, whereas the baryonic matter can account for only 5–6%. The nature of dark matter, and its properties, is completely unknown and so far dark matter particles have evaded direct detection. There are, however, various viable models that could easily be incorporated into what we know of high-energy particle physics.

The models that have been most consistently explored are those in which the dark matter is made of WIMPS most often identified with the lightest symmetry particles in SUSY or SUGRA extensions of the standard models. In this scenario, these particles would be heavy particles produced and decoupled from the baryonic content of the universe in an early stage of its thermal history. Experiments aiming at detecting these particles have been set up. They have been unsuccessful so far but have started exploring the parameter space of these theories. Theorists have explored other possibilities including the axions, light particles that would have been produced through a non-thermal mechanism and whose existence is related to the weak CP violation of the strong interactions or even boson condensates, although in this case no convincing global scenarios have yet been proposed.

The very new picture emerging in recent years is, however, not so much for the existence of dark matter but for a growing set of evidences favouring the existence of a dark energy component. Its observation signature has different aspects. It appears from large-scale structure studies as a missing energy density required to make the spatial curvature of the universe zero, found to be nil from CMB observations, or to account for the effective equation

of state of the cosmic fluid at low redshifts. It should actually be noticed that these two pieces of evidence result from low-redshift effects. From a theoretical point of view the dark energy problem can be viewed from different perspectives. It can be analysed as a geometrical effect and accounted for by a change of the Friedmann equations at the current Hubble scale. In this perspective it should be recalled that the Friedmann equations are probing gravity at the horizon scale, a regime which is just about to be partly testable. The dark energy problem can also be viewed from a high-energy physics point of view. Assuming that GR holds at scales as large as possible, this dark energy should be related to the energy density associated with the cosmological vacuum state. This state, and its properties are far from being trivial from the quantum field theory point of view. If the dark energy observations are to be taken seriously it implies that the late time background state is de Sitter, an uncomfortable situation for any quantum field calculations, unless the observed cosmological vacuum state is only transitory. This is in particular what is advocated in quintessence models.

In none of these points of view, however, are there clues to why the dark energy component, wherever it comes from, should start to play a role precisely now. This coincidence problem is probably one of the most disturbing aspects that the existence of a dark energy raises. The very existence and nature of this component is bound to be a matter of debate in the coming years.

As mentioned before, the dark energy issue is a low redshift effect phenomenon. This is to be brought closer to the new era of precision measurements, which studies of large-scale structure are entering into. This concerns galaxy and weak lensing surveys and to a lesser extent cosmic microwave background experiments. With such surveys precise quantitative tests can be designed where the very details of the model of the structure growth can be scrutinized. Weak lensing surveys are likely to be particularly efficient for testing the late time large-scale structure growth. They can serve to test both the geometrical and energetic aspects of the issue of fundamental physics which the detection of the dark energy component has raised.

References

[1] Ahmad Q R *et al* [SNO Collaboration] 2002 *Phys. Rev. Lett.* **89** 011302 [arXiv:nucl-ex/0204009]
[2] Ahmad Q R *et al* [SNO Collaboration] 2002 *Phys. Rev. Lett.* **89** 011301 [arXiv:nucl-ex/0204008]
[3] Allen S W, Ettori S and Fabian A C 2001 *MNRAS* **324** 877
[4] Arkani-Hamed N, Dimopoulos S and Dvali G 1998 *Phys. Lett.* B **429** 263
Arkani-Hamed N, Dimopoulos S and Dvali G 1999 *Phys. Rev.* D **59** 086004
Antoniadis I *et al* 1998 *Phys. Lett.* B **436** 257
[5] Bacon D, Refregier A and Ellis R 2000 *MNRAS* **318** 625–40
[6] Baugh C M and Gaztañaga E 1996 *MNRAS* **280** L37–41
[7] Benabed K and Bernardeau F 2001 *Phys. Rev.* D **64** 083501
[8] Benoit A *et al* [The Archeops collaboration] astro-ph/0210305
[9] Benoit A *et al* [The Archeops collaboration] astro-ph/0210306
[10] Benoit A *et al* [The Edelweiss collaboration] 2002 *Phys. Lett.* B **545** 43–9
[11] Bernardeau F 1992 *ApJ* **392** 1–14
[12] Bernardeau F 1994 *ApJ* **433** 1–18
[13] Bernardeau F 1995 *A&A* **301** 309–17
[14] Bernardeau F, Mellier Y and van Waerbeke L astro-ph/0201032
[15] Bernardeau F, Van Waerbeke L and Mellier Y 1997 *A&A* **322** 1–18
[16] Bernardeau F, Van Waerbeke L and Mellier Y astro-ph/0201029
[17] Bernardeau F, Colombi S, Gaztañaga E and Scoccimaro R 2002 *Phys. Rep.* **367** 1–128
[18] Bernardeau F and Uzan J-P 2002 *Phys. Rev.* D
[19] Bertschinger E and Dekel A 1989 *ApJ* **336** L5
[20] Binétruy P, Deffayet C and Langlois D 2000 *Nucl. Phys.* B **565** 269
[21] Binétruy P and Silk J [astro-ph/0007452]
[22] Blandford R D, Saust A B, Brainerd T G and Villumsen J V 1991 *MNRAS* **251** 600–27
[23] Bond J R, Cole S, Kaiser N and Efstathiou G 1991 *ApJ* **379** 440–60

[24] Bouchet F R, Colombi S, Hivon E and Juszkiewicz R 1995 *A&A* **296** 575–608
[25] Bouchet F R, Juszkiewicz R, Colombi S and Pellat R 1992 *ApJ* **394** L5–8
[26] Brax Ph and Martin J 2000 *Phys. Rev.* D **61** 103502
[27] Brax Ph and Martin J 1999 *Phys. Lett.* B **468** 40
[28] Brax Ph, Martin J and Riazuelo A 2000 *Phys. Rev.* D **62** 103505
[29] Cooray A and Seth R K astro-ph/0206508
[30] Davé R, Spergel D N, Steinhardt P J and Wandelt B D 2001 *ApJ* **547** 574–89
[31] Davis M, Efstathiou G, Frenk C S and White S D M 1985 *ApJ* **292** 371–94
[32] Deffayet C, Dvali G and Gabadadze G 2002 *Phys. Rev.* D **65** 044023
[33] Dekel A 1994 *ARA&A* **32** 371
[34] Eke V R, Cole S and Frenk C S 1996 *MNRAS* **282** 263–80
[35] Elgaroy O *et al* 2002 for the 2dF galaxy Redshift Survey *Phys. Rev. Lett.* **89** 061301
[36] Ferreira P G and Joyce M 1998 *Phys. Rev.* D **58** 023503
[37] Fry J N 1984 *ApJ* **279** 499–510
[38] Fry J N 1994 *Phys. Rev. Lett.* **73** 215–19
[39] Fry J N and Gaztañaga E 1993 *ApJ* **413** 447–52
[40] Fry J N and Seldner M 1982 *ApJ* **259** 474–81
[41] Fukuda S *et al* [Super-Kamiokande Collaboration] 2001 *Phys. Rev. Lett.* **86** 5656 [arXiv:hep-ex/0103033]
[42] Garriga J and Tanaka T 2000 *Phys. Rev. Lett.* **84** 2778
Chung D J, Everett L and Davoudias H [hep-ph/0010103]
[43] Gaztañaga E and Baugh C M 1998 *MNRAS* **294** 229–44
[44] Gaztanaga E and Lobo A 2001 *ApJ* **548** 47–59
[45] Goroff M H, Grinstein B, Rey S-J and Wise M B 1986 *ApJ* **311** 6
[46] Gregory R, Rubakov V A and Sibiryakov S M [hep-th/0002072].
[47] Guth A H 1981 *Phys. Rev.* D **23** 347–56
[48] Guth A H and Pi S-Y 1985 *Phys. Rev.* D **32** 1899–920
[49] Hamuy M *et al* 1993 *AJ* **106** 2392
[50] Halverson N W *et al* 2002 *ApJ* **568** 38
[51] Hamilton A J S, Kumar P, Lu E and Matthews A 1991 *ApJ* **374** L1
[52] Hivon E, Bouchet F R, Colombi S and Juszkiewicz R 1995 *A&A* **298** 643–60
[53] Hu W 1995 *PhD Thesis* University of California at Berkeley, see also http://background.uchicago.edu/ whu/
[54] Hui L 1999 *ApJ* **519** L9–12
[55] Huterer D 2001 astro-ph/0106399
[56] Jain B and Bertschinger E 1994 *ApJ* **431** 495–505
[57] Jain B and Seljak U 1997 *ApJ* **484** 560–73
[58] Kaiser N 1992 *ApJ* **388** 272–86
[59] Kaiser N and Squires G 1993 *ApJ* **404** 441
[60] Kaiser N 1995 *ApJ* **439** 1
[61] Kaiser N, Wilson G and Luppino G A 2000 astro-ph/0003338
[62] Kiefer C, Polarski D and Starobinsky A A 1998 *Int. J. Mod. Phys.* D **7** 455–62
[63] Kiefer C, Lesgourgues J, Polarski D and Starobinsky A A 1998 *Class. Quant. Grav.* **15** L67–72
[64] Kogan I I *et al* [hep-ph/9912552]
[65] Kolb E W and Turner M S 1993 *The Early universe* (New York: Addison-Wesley)
[66] Lee A T *et al* 2001 *ApJ* **561** L1
[67] Liddle A R and Lyth D H 1993 *Phys. Rep.* **231** 1–105
[68] Liddle A R and Lyth D H 2000 *Cosmological Inflation and Large-Scale Structure* (Cambridge, UK: Cambridge University Press)
[69] Lyth D H and Riotto A 1999 *Phys. Rev.* D **59** 103503
[70] Maddox S J, Efstathiou G, Sutherland W J and Loveday J 1990 *MNRAS* **242** 43
[71] Makino N, Sasaki M and Suto Y 1992 *Phys. Rev.* D **46** 585–602
[72] Maoli *et al* 2001 *A&A* **368** 766
[73] Mather J C *et al* 1990 *ApJ* **354** L37–40
[74] Mellier Y 1999 *ARA&A* **37** 127–89
[75] Miralda-Escudé J 1991 *ApJ* **380** 1–8
[76] Mukhanov V F, Feldman H A and Brandenberger R H 1992 *Phys. Rep.* **215** 203
[77] Narayanan V, Berlind A and Weinberg D 2000 *Astrophys. J.* **528** 1
[78] Netterfield C B *et al* 2002 *ApJ* **571** 604
[79] Peacock J A *et al* for the 2dF galaxy Redshift Survey, astro-ph/0204239

[80] Peacock J A and Dodds S J 1996 *MNRAS* **280** L19
[81] Peccei R D and Quinn H R 1977 *Phys. Rev. Lett.* **38** 1440–3
[82] Peebles P J E 1980 *The Large-Scale Structure of the universe* (Princeton, NJ: Princeton University Press)
[83] Perlmutter S *et al* 1999 *ApJ* **517** 565
[84] Pierre M, Le Borgne J F, Soucail G and Kneib J-P 1996 *A&A* **311** 413
[85] Press W H and Schechter P 1974 *ApJ* **187** 425–38
[86] Randall L and Sundrum R 1999 *Phys. Rev. Lett.* **83** 3370
Randall L and Sundrum R 1999 *Phys. Rev. Lett.* **83** 4690
[87] Ratra B and Peebles P J E 1988 *Phys. Rev.* D **37** 3406
[88] Sachs R K 1961 *Proc. R. Soc.* A **264** 309–38
[89] Saini T D, Raychaudhury S, Sahni V and Starobinsky A A 2000 *Phys. Rev. Lett.* **85** 1162
[90] Schneider P and Lombardi M 2002 astro-ph/0207454
[91] Smoot G *et al* 1992 *ApJ* **396** L1
Bennett C L *et al* 1996 *ApJ* **464** L1
[92] Soucail G, Mellier Y, Fort B, Mathez G and Cailloux M 1988 *A&A* **191** L19
[93] Spergel D N and Steinhardt P J 2000 *Phys. Rev. Lett.* **84** 3760–3
[94] Squires G, Kaiser N, Babul A, Fahlman G, Woods D and Neumann D M and Böhringer H 1996 *ApJ* **461** 572
[95] Steinhardt P J, Wang L and Zlatev I 1999 *Phys. Rev.* D **59** 123504
[96] Strauss M astro-ph/9908325 *Proc. Cosmic Flows Workshop (Victoria, Canada, July 1999)* ed S Courteau *et al* ASP Series at press
[97] Takada M and Jain B 2002 astro-ph/0210261
[98] Tegmark M *et al* 1996 *ApJ* **464** L35
[99] Tegmark M and Zaldarriaga M 2002 astro-ph/0207047
[100] Uzan J-P and Bernardeau F 2001 *Phys. Rev.* D **64** 083004
[101] van Waerbeke L *et al* 2000 *A&A* **358** 30
[102] van Waerbeke L *et al* 2001 *A&A* **374** 757
[103] van Waerbeke L, Hamana T, Scoccimarro R, Colombi S and Bernardeau F 2001 *MNRAS* **322** 918–26
[104] Villumsen J V 1996 *MNRAS* **281** 369–83
[105] Wittman D M, Tyson J A, Kirkman D, Dell'Antonio I and Bernstein G 2000 *Nature* **405** 143–8
[106] Yoshida N, Springel V, White S D M and Tormen G 2000 *ApJ* **544** L87–90
[107] Zaldarriaga M and Scoccimarro R 2002 astro-ph/0208075
[108] Zwicky F 1938 *Pub. Astr. Soc. Pac.* **50** 218–20
[109] see the CFHLS web site, http://www.cfht.hawaii.edu/Science/CFHLS/
[110] see http://snap.lbl.gov/
[111] see http://chandra.harvard.edu/photo/category/galaxyclusters.html
[112] see http://xmm.vilspa.esa.es/external/xmm_science/1st_results/index.shtml